iScience

CellPress
OPEN ACCESS

Article

Vitamin D sufficiency enhances differentiation of patient-derived prostate epithelial organoids

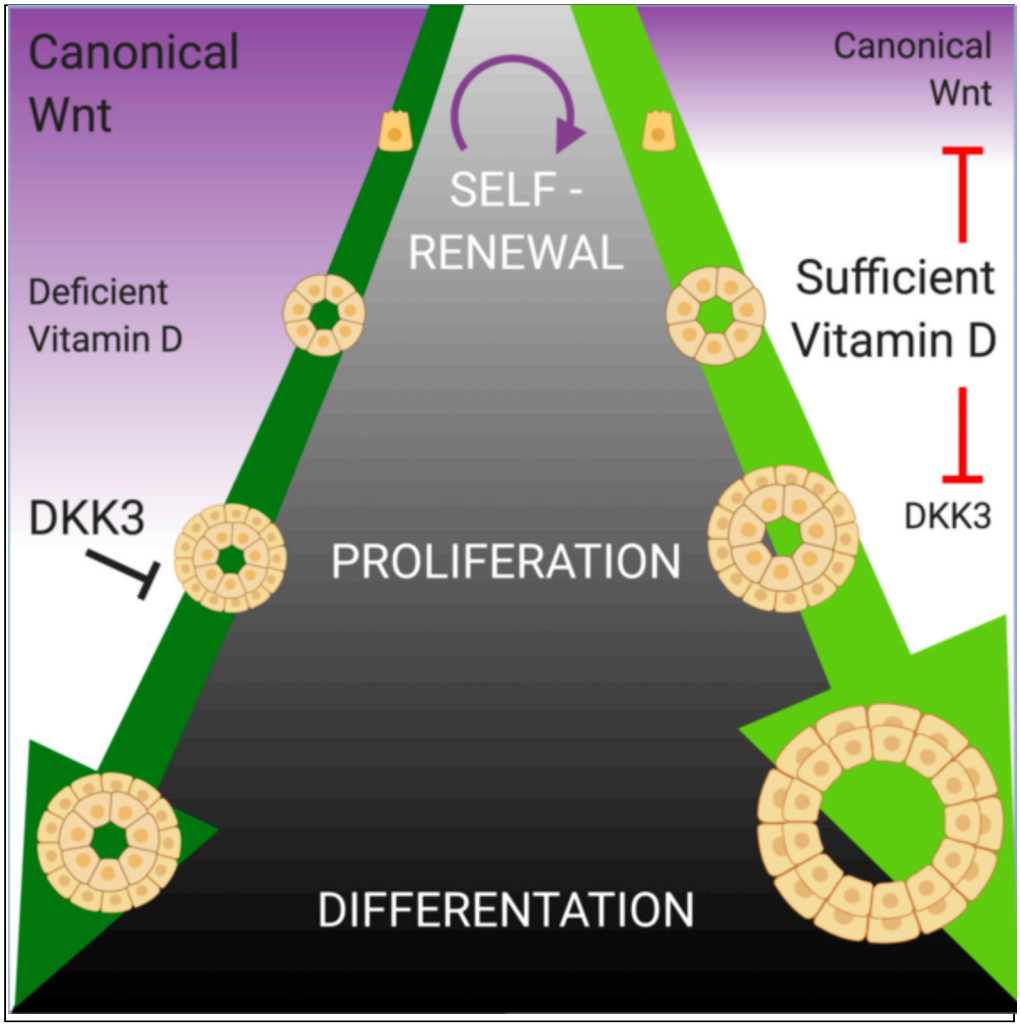

Tara McCray, Julian V. Pacheco, Candice C. Loitz, ..., Klara Valyi-Nagy, Michael R. Abern, Larisa Nonn

lnonn@uic.edu

Highlights

Vitamin D sufficiency accelerates differentiation of patient-derived prostate organoids

Single-cell RNAseq of organoids reveals differentiation trajectory over time

Vitamin D inhibits canonical Wnt activity in human prostate organoids and explants

Inhibition of DKK3 by vitamin D promotes organoid growth and proliferation

McCray et al., iScience 24, 101974
January 22, 2021
https://doi.org/10.1016/j.isci.2020.101974

iScience

CellPress
OPEN ACCESS

Article

Vitamin D sufficiency enhances differentiation of patient-derived prostate epithelial organoids

Tara McCray,[1] Julian V. Pacheco,[1] Candice C. Loitz,[1] Jason Garcia,[1] Bethany Baumann,[1] Michael J. Schlicht,[1,2] Klara Valyi-Nagy,[1,2] Michael R. Abern,[2,3] and Larisa Nonn[1,2,4,*]

Summary

Vitamin D is an essential steroid hormone that regulates systemic calcium homeostasis and cell fate decisions. The prostate gland is hormonally regulated, requiring steroids for proliferation and differentiation of secretory luminal cells. Vitamin D deficiency is associated with an increased risk of lethal prostate cancer, which exhibits a dedifferentiated pathology, linking vitamin D sufficiency to epithelial differentiation. To determine vitamin D regulation of prostatic epithelial differentiation, patient-derived benign prostate epithelial organoids were grown in vitamin D-deficient or -sufficient conditions. Organoids were assessed by phenotype and single-cell RNA sequencing. Mechanistic validation demonstrated that vitamin D sufficiency promoted organoid growth and accelerated differentiation by inhibiting canonical Wnt activity and suppressing Wnt family member DKK3. Wnt and DKK3 were also reduced by vitamin D in prostate tissue explants by spatial transcriptomics. Wnt dysregulation is a known contributor to aggressive prostate cancer, thus findings further link vitamin D deficiency to lethal disease.

Introduction

Vitamin D is a misnomer as it is not a vitamin, but rather a vital steroid, synthesized in the skin following UV exposure. Circulating pro-hormone is further metabolized to the active hormone calcitriol (1,25-dihydroxyvitamin D [1,25D]) which controls systemic calcium homeostasis and locally regulates cell fate decisions. In target cells, 1,25D binds to the vitamin D receptor (VDR), a classical steroid hormone receptor that associates with vitamin D response elements on DNA to control gene expression (Feldman et al., 2014). Vitamin D regulates at least 3% of the genome (Bouillon et al., 2008) and chromatin immunoprecipitation (ChIP) sequencing for VDR-bound DNA in prostate epithelial cells revealed binding at more than 3,000 protein-coding genes, and over 1,000 noncoding sites (Baumann et al., 2019; Fleet et al., 2019). Genes regulated by vitamin D are involved in proliferation, differentiation, and apoptosis pathways (Feldman et al., 2014). Vitamin D metabolites are pro-differentiating in a variety of cell and tissue types, including keratinocytes (MacLaughlin et al., 1990), intestinal villi (Peregrina et al., 2015; Spielvogel et al., 1972), cardiomyocytes (Hlaing et al., 2014), odontoblasts (Mucuk et al., 2017), placenta (Hutabarat et al., 2018), and macrophages (Abe et al., 1981; James et al., 1997). Some of these studies explore 1,25D action in benign cells, whereas the majority of reports focus on vitamin D inhibition of cancer cell growth and tumor progression (Aguilera et al., 2007; Banks and Holick, 2015; Holick et al., 2007; Larriba et al., 2011; Tavera-Mendoza et al., 2017; Yang et al., 2017), and very little is known about the pro-differentiating activity of vitamin D in benign prostate.

Other hormones are essential for prostate differentiation; retinoic acid regulates prostate bud formation during development (Bryant et al., 2014) and androgen regulates terminal differentiation of luminal epithelial cells (Prins and Lindgren, 2015; Wright et al., 1996). The prostate has robust expression of VDR and the enzymes required for local production of 1,25D from the circulating pro-hormone, 25-hydroxyvitamin D (Peehl et al., 2004), indicating that the hormone vitamin D is active in the gland as well. The benign prostate of castrated rats supplemented with androgen and 1,25D showed increased number of secretory vesicles in regenerated luminal cells compared with androgen alone (Konety et al., 1996), supporting improved differentiation with vitamin D. In prostate cancer (PCa) cell lines, treatment with a vitamin D analog increased

[1]Department of Pathology, University of Illinois at Chicago, 840 S Wood Street, Chicago, IL 60612, USA

[2]University of Illinois Cancer Center, Chicago, IL 60612, USA

[3]Department of Urology, University of Illinois at Chicago, Chicago, IL 60612, USA

[4]Lead contact

*Correspondence: lnonn@uic.edu

https://doi.org/10.1016/j.isci.2020.101974

E-cadherin expression (Campbell et al., 1997). Although these two studies suggest that vitamin D enhanced prostatic differentiation by expression of a more "normal" phenotype, the mechanism was not determined.

Hormone dysregulation, such as androgen and androgen receptor, contributes to PCa initiation and progression (Karantanos et al., 2013). Similar observations have been made for vitamin D and VDR; well-differentiated prostate tumors have high VDR expression, whereas high Gleason grade, poorly differentiated tumors have low VDR expression (Hendrickson et al., 2011). The relationship between vitamin D dysregulation and aggressive disease is supported by rodent models, where prostatic VDR deletion within the TgAPT mouse model of prostate carcinogenesis increased adenocarcinoma foci number and area (Fleet et al., 2019). The relationship is also observed in patients, where vitamin D deficiency is associated with risk of aggressive PCa (Fang et al., 2011; Giovannucci et al., 2006; Murphy et al., 2014; Ramakrishnan et al., 2019; Studzinski and Moore, 1995). Vitamin D deficiency is especially pertinent to patients with PCa who are frequently deficient due to high skin melanin content, such as African Americans (Murphy et al., 2014), or lack of sun exposure (Gilbert et al., 2009), such as the elderly (Elshazly et al., 2017). This observation was originally identified as distance from the equator increasing the risk of PCa mortality (Hanchette and Schwartz, 1992; Studzinski and Moore, 1995) and diagnosis during summer improving PCa prognosis (Robsahm et al., 2004). Clinical trials using vitamin D supplementation in patients with existing PCa have had both promising (Marshall et al., 2012; Woo et al., 2005) and null results (Chandler et al., 2014). However, patients with PCa are known to have low expression of VDR (Hendrickson et al., 2011) supporting that vitamin D supplementation is more useful as a chemopreventive agent rather than as a PCa treatment. Recently, the VITAL study assessed 2000 IU/day vitamin D supplementation in healthy subjects to explore cancer incidence and found a decreased risk of cancer in the normal body mass index group (Manson et al., 2019).

Given the reliance of the prostate on hormone signaling for differentiation, the high activity of the hormone vitamin D in the gland, and the association of vitamin D deficiency with risk of aggressive PCa (Murphy et al., 2014), we hypothesized that vitamin D promotes prostatic epithelial differentiation and that its deficiency contributes to the loss of epithelial homeostasis observed in aggressive PCa. To explore the effects of deficient and sufficient 1,25D on prostate epithelium, patient-derived organoids were used to model epithelial differentiation (Drost et al., 2016) in physiologically relevant levels of the hormone. We previously optimized culture conditions for clonal growth of organoids from single cells (Richards et al., 2019) and characterized prostate organoids using single-cell RNA sequencing (scRNAseq) (McCray et al., 2019).

Results

Sufficient 1,25D supports growth of benign patient-derived prostate epithelial organoids

To determine the effect of 1,25D on organoid phenotype, we grew organoids derived from a benign region of radical prostatectomy tissue from a single patient in media supplemented with 10 nM 1,25D, 50 nM 1,25D (vitamin D-sufficient), or vehicle control (vitamin D-deficient, <0.01% EtOH) (Figure 1A). VDR was found to be expressed in all patient-derived PrE cells examined (Figure S1A), including patient AA2. The clonal origin of organoids within this model has been previously demonstrated by our group through time-lapse microscopy studies and lineage tracing with fluorescent proteins (Richards et al., 2019). Similar to other reports (Barros-Silva et al., 2018; Wang et al., 2015a), we observed organoids with heterogeneous morphologies that include solid spheres and acinar/tubule-like structures, with a small percentage of translucent spheres (Figure 1A). Both concentrations of 1,25D produced visibly larger organoid areas compared with the vitamin D-deficient control organoids (Figure 1A). The 10 nM dosage was selected for subsequent studies, as it strongly upregulated the VDR-response gene *CYP24A1* (Chen and DeLuca, 1995; Zierold et al., 1995) (Figure S1B) and is a biologically relevant concentration, equivalent to ~4 ng/mL vitamin D (circulating levels of active and inactive forms in serum are 50 pg/mL and 40 ng/mL, respectively) (Richards et al., 2017). Studies were expanded to include a larger and more diverse group of 10 patient-derived PrE cells (Table 1). Vitamin D sufficiency increased the percentage of translucent and acinar organoids, which are considered more differentiated morphologies (Figure 1B). Organoid size was significantly increased by 1,25D (Figures 1C and 1D, Table 1). The magnitude of the 1,25D-induced size increase varied between patients, highlighting the model's preservation of patient heterogeneity (Figures 1C and 1D). Flow cytometry of day 14 organoids for luminal cell marker CD26 (Henry et al., 2018) and basal-progenitor colony-forming cell marker CD49f (Yamamoto et al., 2012) revealed a noticeable shift in CD49f cells at day 14 with 1,25D treatment (blue) when compared with control (red) (Figure 1E). Overall, sufficient 1,25D

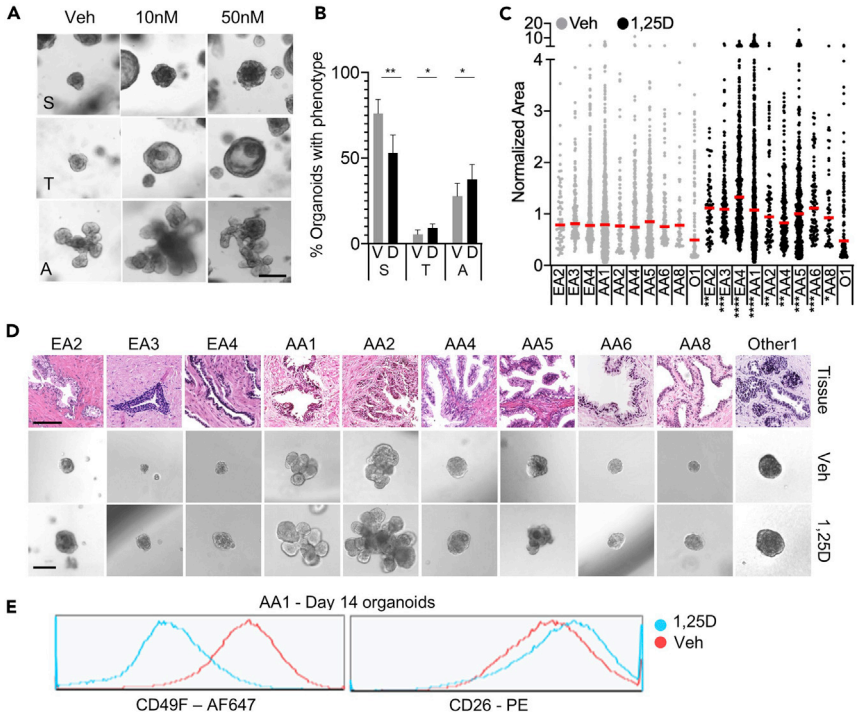

Figure 1. Sufficient 1,25D supports growth of benign patient-derived prostate epithelial organoids

(A) AA2 organoids grown in vehicle (Veh, <0.01 % EtOH) or 10 nM or 50 nM 1,25D until day 23. Three representative images are shown for each condition to illustrate heterogeneity of organoid morphology: solid (S), translucent (T), and acinar (A) structures were observed. Scale bar, 200 μm.

(B) Percentage of organoids with phenotype after culture in deficient 1,25D (V, vehicle), or sufficient 1,25D (D, 10 nM 1,25D). Solid (S), translucent (T), and acinar (A) organoids were counted per well in n ≥ 3 wells for 10 patients, and the percentage of each were calculated. Organoids derived from 7 patients were capable of forming all three types of morphologies; only those percentages were averaged and reported here. Error bars represent the standard error of the mean. (*p < 0.1; **p < 0.05).

(C) Relative area of PrE organoids grown in vehicle (Veh) or 10 nM 1,25D (1,25D) for approximately 14 days, showing ≥3 replicate wells per patient for each condition, repeated 1–4 times per patient as listed in Table 1. Area is normalized to the mean of the vehicle per patient per experiment; each dot represents an organoid. Patients represent biological replicates. (AA, African American; EA, European American; O, Other, not African or European descent, ancestries were patient self-declared; *p < 0.1; **p < 0.05; ***p < 0.01, ****p < 0.001).

(D) Representative images of day 14 organoids grown in deficient (Veh, middle) or sufficient vitamin D (10 nM 1,25D, lower) and corresponding H&E staining for patient tissue from which organoids were derived (upper); scale bar: 200 μm for organoids and 100 μm for tissue.

(E) Overlay of flow histograms for luminal marker CD26 (right) and basal-progenitor marker CD49f (left) in AA1 organoids grown until day 14 in vehicle (red, Veh) or 10 nM 1,25D (blue, 1,25D).

See also Figure S1.

significantly increased organoid size and morphology and promoted differentiation away from a CD49f basal-progenitor phenotype, indicating improved growth with vitamin D.

Epithelial populations in primary prostate cell organoids by scRNAseq

Having established a 1,25D-induced phenotype of increased size across multiple patient-derived organoids (Figure 1), we next determined how 1,25D affected the epithelial populations within the organoids over time. Control and 1,25D-sufficent organoids from patient AA2 were collected for scRNAseq at two time points along the differentiation spectrum: day 8 and day 14 (Figure 2A, left). AA2 was selected due to availability of cells from this patient, capacity for these cells to form acinar organoids, and response to 1,25D. Target 1,25D genes and pathways identified by the scRNAseq in AA2 were later validated in additional patients' cells. Seurat version 3 was used to integrate datasets, align similar cells found in each sample, generate clusters, and perform differential expression analysis (Butler et al., 2018; Satija et al., 2015); the resulting UMAP of the integrated dataset and distribution of epithelial clusters found in each sample are

Table 1. Patient characteristics

Patient[a]	Age at RP[b]	Pathology	Fold change of organoid area with 1,25D	Significance of organoid area with 1,25D[c]	# Of Aliquots tested per patient	# Of replicate wells per condition
EA1	59	Benign	NA[d]	NA		
EA2	?	Benign	***1.41***	***0.0313***	1	3
EA3	57	Benign	***1.345***	***0.0011***	2	6
EA4	60	Benign	***1.708***	***<0.0001***	3	9
AA1	71	Benign	***1.359***	***<0.0001***	4	12
AA2	68	Benign	***1.22***	***0.0142***	1	3
AA3	72	Benign	NA	NA		
AA4	58	Benign	***1.1119***	***0.0251***	2	6
AA5	60	Benign	***1.182***	***0.0019***	2	6
AA6	50	Benign	***1.47***	***0.0007***	2	6
AA8	58	Benign	***1.189***	***0.0536***	1	3
AA9	?	Benign	NA	NA		
Other1	58	Benign	0.9680	0.4616	1	3

Significant values are bold and italics.
[a]EA, European American; AA, African American; Other, non-European or African descent.
[b]RP, radical prostatectomy.
[c]Non-parametric one-tailed Mann-Whitney test.
[d]NA, patient not used for organoid area assay.

shown (Figure 2A, middle and right). Cluster markers were determined by unbiased identification of genes that had uniquely high or low expression in each cluster (Figures 2B and S2A) and were input into Ingenuity Pathway Analysis (IPA) software to identify canonical pathways enriched in each population (Kramer et al., 2014) (Figure S2B), as described below. To name the clusters, the expression of specific previously identified epithelial markers was interrogated and visualized by dot plot (Figure 2C), which shows the percentage of cells in each cluster that express the marker of interest, and how high or low that expression is relative to the other cells in the dataset.

Resident, quiescent stem cells were identified by high expression of *KRT13* (Henry et al., 2018; Hu et al., 2017) (Figures 2B and 2C). This cluster had the most distinct expression profile with the highest number of markers (Figure S2A). By IPA, the *KRT13* stem cell population had specific activation of the Wnt/β-catenin and VDR/RXR pathways, similar to what has been reported in the gut and skin stem cells (Bikle, 2004; Peregrina et al., 2015) (Figure S2B, red asterisks). Downstream progenitors were marked by modest *KRT13* expression but high expression of the progenitor marker *KRT6A* (Schmelz et al., 2005), along with expression of basal markers *KRT5/KRT14*, intermediate marker *KRT19* ((Wang et al., 2001)), and *TACSTD2*, which codes for the stem cell marker Trop2 (Goldstein et al., 2008) (Figures 2B and 2C). A luminal phenotype was distinguished by expression of *KRT8/KRT18* and *DPP4* (CD26) (Figure 2C). However, transcripts for *DPP4* were low and do not reflect the protein expression of CD26 observed by flow cytometry. Two basal populations were identified by *KRT5*, *KRT14*, *TP63*, and *PDPN* (Henry et al., 2018) (Figure 2C). Dividing cells were recognized by cell division markers *CENPF*, *MKI67*, *TOP2A*, *PCNA*, *MCM7*, *CCNB1*, and *HIST1H4C* (Figure 2C). The "Integrin^{High}" population was identified based on integrin expression (*ITGB6*, *ITGB4*), expression of integrin-binding partner *FN1*, and other adhesion junction proteins (*DST*, *CD44*, Figures 2B and 2C) (Ryan et al., 2012; Sneath and Mangham, 1998). Markers for the Integrin^{High} cluster were enriched for the HIPPO pathway, which regulates contact inhibition of polarized cell types (Genevet and Tapon, 2011) (Figure S2, red asterisks). These cells may be starting to polarize through integrin interactions with the basement-membrane-protein ligands found in the Matrigel.

Immunostaining of organoids confirmed protein expression for major cluster markers (Figure 2D, single channels shown in Figure S3). Basal proteins CK5 and p63 were expressed along the periphery of the organoid (Figure 2D, upper left and right, green arrowhead). Although AR mRNA transcripts were low in the dataset, AR^{+} luminal cells were observed by immunohistochemistry (IHC) (Figure 2D, upper middle, black arrowhead). The luminal marker

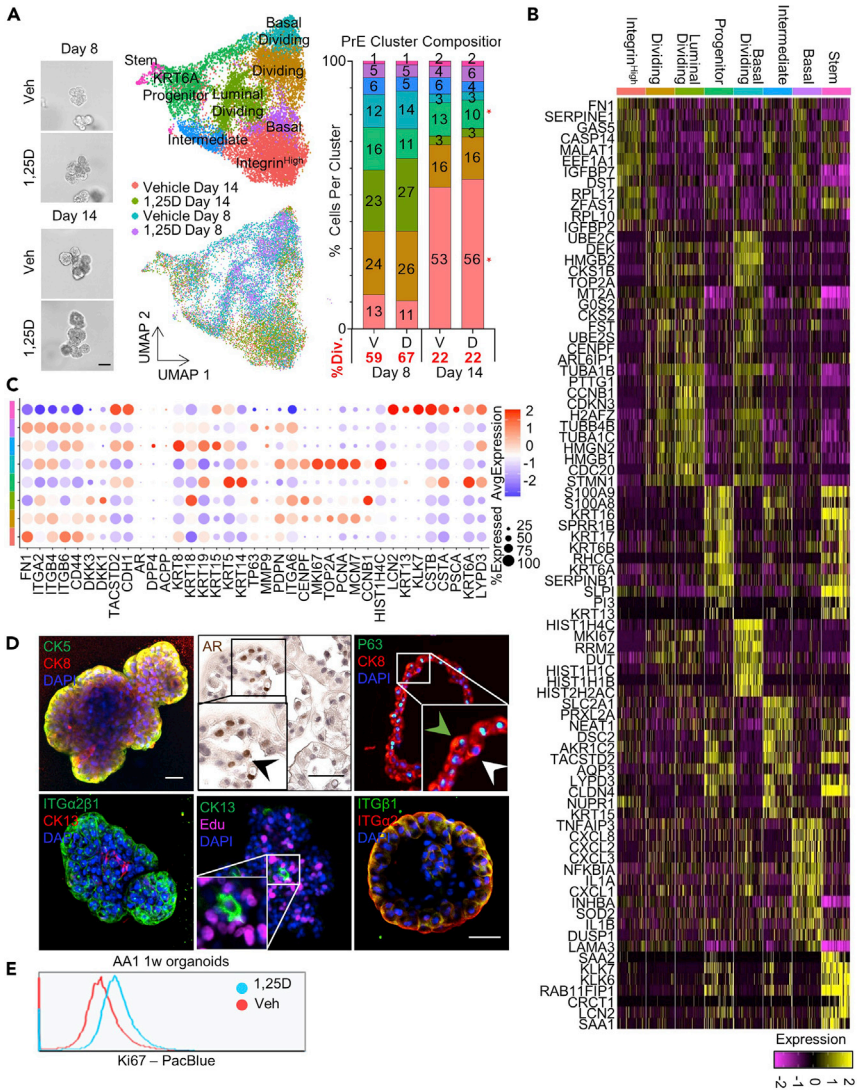

Figure 2. Epithelial populations in primary prostate cell organoids by scRNAseq

(A) Representative images of the AA2 organoids grown in vehicle (Veh) or 10 nM 1,25D (1,25D) collected at day 8 and day 14 for scRNAseq (left). Scale bar, 100 μm. UMAP of integrated scRNAseq data for vehicle and 1,25D samples at day 8 and day 14 (middle), showing clustering (upper) and distribution of samples (lower). Bar chart depicting the percentage of cells per cluster in each sample, vehicle (V) and 1,25D (D), at each time point (right); percentage of total dividing (%Div.) cells is shown in red text.

(B) Heatmap of cluster markers for integrated scRNAseq dataset shown in (A). Cluster markers were identified by Seurat as genes having uniquely high or low expression in each cluster, compared with all other cells in the dataset.

(C) Dot plot showing expression of specific epithelial markers in each cell cluster. The size of dots represents the percentage of cells in each cluster that express the gene, and the color represents relative expression of the cells in that cluster compared with all remaining cells.

(D) Immunostaining of formalin-fixed, paraffin-embedded organoids (upper middle and right) and whole-mounted organoids (remaining panels). Staining for luminal makers CK8 and AR; basal markers CK5 and P63; stem cell marker CK13; polarization markers ITGα2β1, ITGα2, and ITGβ1; and incorporation of EdU are shown. Black and white arrow heads indicate AR+/P63- luminal cells. Green arrowhead indicates P63+ cell. Scale bar, 50 μm. Single channels for each condition included in Figures S3.

(E) Overlay of flow cytometry histogram for proliferation marker Ki67 in AA1 organoids grown until day 7 in vehicle (red, Veh) or 10 nM 1,25D (blue, 1,25D).

See also Figures S2–S4.

CK8/18 was highly expressed by most cells in the organoids, but there were $p63^{-}/CK8^{+}$ cells indicating a continuum of basal-intermediate-luminal cells in the organoids (Figure 2D, upper left and right, white and green arrowheads). This was also observed in the scRNAseq data where 100% of cells in every clusters express KRT8 (Figure 2C), but at different relative levels between the clusters. A $CK13^{+}$ stem cell identified in an organoid was negative for EdU incorporation after briefly pulsing overnight with EdU before staining (Figure 2D, lower middle), supporting its quiescence. Integrin subunits α2 and β1 and heterodimer integrin α2β1 were observed at the organoid-Matrigel interface where they are likely binding collagen and laminins found in the Matrigel to direct cell polarity (Figure 2D, lower left and right). $CK13^{+}$ cells were negative for integrin α2/β1, demonstrating separation between the stem and $Integrin^{High}$ clusters. In sum, these results confirm differentiation of a heterogeneous population of epithelial cells sharing markers identified by scRNAseq.

Once clusters were identified, population shifts over time and with vitamin D were explored using Fisher's exact test (Figure S4, p value shown inset in the heatmap). Early-stage day 8 organoids consisted primarily of dividing cell types, indicative of rapid cellular expansion in culture and significantly different when compared with day 14 organoids (Figure 2A, red text, Figure S4A). After differentiation at day 14, there was significant enrichment in the $Integrin^{High}$ polarized cells compared with day 8. Culture in sufficient 1,25D increased the percentage of dividing cells at day 8 from 59% to 67% of the cell population (Figure 2A, red text), which was significant (Figure S4B) and validated by flow cytometry for KI67 (Figure 2E). At day 14, population shifts with 1,25D were modest but significant (Figure S4C), with a slight increase in the number of polarized and basal cells and a decrease in the number of progenitor and intermediate cells (Figure 2A, red asterisks). The data support that 1,25D promotes both growth and differentiation through enrichment of dividing cells at day 8 and $Integrin^{High}$ cells at day 14.

1,25D modulates the Wnt pathway in organoids

Like most hormones, vitamin D is pleiotropic and regulates many pathways in prostate cells. To determine the action of 1,25D in organoids, differentially expressed genes (DEGs) after culture in 1,25D compared with vehicle in each cluster at each time point were explored (Figure S5A). Of note, the stem cells had the fewest DEGs with 1,25D, indicating a stable transcriptional program. DEGs were input into IPA software to identify enriched Canonical Pathways (Figures 3A and S5B), Upstream Regulators (Figure S6), and their Downstream Effects (Figure S7) (Kramer et al., 2014).

Significantly enriched canonical pathways in all clusters included VDR/RXR activation (Figure S5B), driven by the highly 1,25D-regulated genes *CYP24A1* and *IGFBP3* (Figure S5B, upper red box) (Martin and Pattison, 2000; Zierold et al., 1995). Examination of pathways related to "Organismal Growth & Development" (Figure 3A) showed enrichment of the BMP and Wnt pathways in 1,25D-sufficient organoids, known regulators of prostate development and differentiation (Toivanen and Shen, 2017). DEGs within the Wnt/β-catenin signaling pathway included upregulation of *DKK1* at day 8 and downregulation of *DKK3* at day 14 (Figure 3A, lower red box). Stem cells showed the fewest number of DEGs with 1,25D culture (Figure S5A), and this cluster showed no enrichment for pathways related to "Organismal Growth & Development." Vitamin D status did not alter the stem population viability as shown by three passages of self-renewal assays in four patients (Figure S5C). Together, this indicates that 1,25D mainly regulates lineage-committed cells on the path to differentiation and does not alter the stable transcriptional program in the stem cells, although these findings were not formally demonstrated by following the progeny of flow-isolated CK13+ cells.

Upstream Regulator analysis predicted active transcription factors, which may have influenced DEG expression. Activation of Vitamin D3-VDR-RXR and cell-type-specific regulation by CTNNB1 (β-catenin) were among the top regulators (Figure S6, red asterisks), confirming vitamin D function and further supporting Wnt/β-catenin involvement. To understand the net effect of the Pathway and Regulator analysis, downstream Disease & Function analysis was performed (Figure S7). Consistent with the hypothesis, there was enrichment for "Differentiation of Epithelial Tissue" at both time points with sufficient 1,25D (Figure S7, red box). The Wnt pathway was selected for additional investigation in the primary prostate cells because previous studies in the RWPE1 prostate cell line, gut, skin, and heart have shown 1,25D inhibition of canonical Wnt signaling (Aguilera et al., 2007; Hlaing et al., 2014; Kovalenko et al., 2010; Larriba et al., 2011; Muralidhar et al., 2019).

Wnt regulation by 1,25D was validated with a targeted RT-qPCR array (Figure 3B). Before RNA isolation, organoids cultured with 10 nM 1,25D or vehicle were sorted by high or low CD49f (Guo et al., 2012; Yamamoto et al., 2012) in an attempt to preserve differences in transcription between progenitor versus

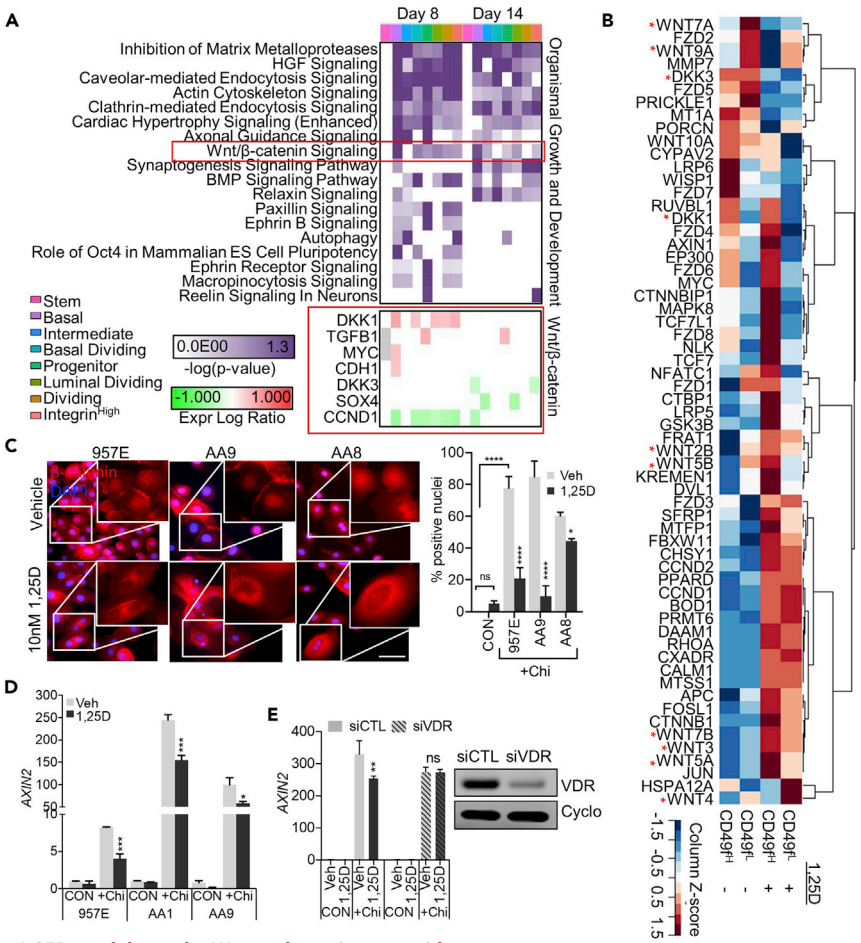

Figure 3. 1,25D modulates the Wnt pathway in organoids

(A) Enriched pathways related to "Organismal Growth and Development" with 1,25D treatment in each cluster at each time point. Differentially expressed genes (DEGs) with 1,25D treatment per cluster were input into IPA Canonical Pathway analysis; pathways related to "Organismal Growth & Development" are shown. Scale represents significance, –log(p value), for enrichment of each pathway with 1,25D. Dark purple is significant at $p < 0.05$. Red box shows DEGs related to Wnt/β-catenin signaling with 1,25D treatment in each cluster. Scale represents the log ratio with 1,25D compared with control.

(B) RT-qPCR array for Wnt pathway gene expression in flow-sorted day 17 AA3 organoids grown in vehicle or 10 nM 1,25D. Cells were sorted by $CD49^{High}$ ($CD49f^{H}$) or $CD49^{Low}$ ($CD49f^{L}$). Log2 of RQ values are shown, normalized to average of housekeeper genes. Hierarchical clustering was performed by Pearson correlation for row and by Spearman for column. Red astericks indicate Wnt ligands and DKK family members.

(C) β-catenin protein localization in 1,25D-treated prostate epithelial cells. Monolayer PrE from two patients (middle and right panel) and benign 957E (left panel) cells grown for 48 or 96 h, respectively, with vehicle or 10 nM 1,25D. Cells were treated with 9 μM Chiron for 5 h, followed by immunostaining for β-catenin (red) and counterstaining with DAPI (blue). Scale bar, 50 μm. Quantification of the percentage of positive nuclei is shown (right); error bars represent the standard deviation of two fields of view. The average of the −Chiron controls (CON, treated with DMSO) is shown to illustrate significant nuclear β-catenin induction upon Chiron treatment (AA8 CON was not collected). p value represents outcome of paired two-way ANOVA with uncorrected Fisher's comparison by row for vehicle versus 1,25D, and for CON versus 957E Chiron Veh. (ns = not significant, *$p < 0.05$, ****$p < 0.0001$).

(D) RT-qPCR of *AXIN2* expression in monolayer PrE cells and benign 957E cells grown and treated as in (C). Relative quantitation is normalized to *HPRT1*. Error bars represent standard deviation of technical RT-qPCR pipetting replicates. Cells from three sources serve as biological replicates. p value represents outcome of paired two-way ANOVA with uncorrected Fisher's comparison by row for vehicle versus 1,25D (*$p < 0.05$; ***$p < 0.001$).

(E) RT-qPCR of *AXIN2* expression (left) in monolayer AA1 PrE cells transfected with siCTL (solid bars) or siVDR RNA (hatched bars) and grown as described in (C). Relative quantitation is normalized to *HPRT1*. Error bars represent standard deviation of technical RT-qPCR pipetting replicates. p value represents outcome of paired two-way ANOVA with uncorrected Fisher's comparison by row for vehicle versus 1,25D. Western for VDR in siCTL and siVDR samples (right) with housekeeper cyclophilin-B (cyclo); full Western blot included in Figure S8C.

See also Figures S4–S8.

lineage-committed cells or basal versus luminal cells, respectively. The expression of multiple canonical and non-canonical Wnts were altered by 1,25D, in some cases in a CD49f-cell-type-specific manner, including *WNT7A, WNT9A, WNT2B, WNT5B, WNT7B, WNT3, WNT5A,* and *WNT4*. Notably, *DKK3* was downregulated with 1,25D treatment in both high ($CD49f^{H}$) and low cells ($CD49f^{L}$) (Figure 3B, red asterisks).

To determine overall directionality of Wnt regulation by 1,25D, β-catenin translocation and *AXIN2* induction were assessed. The GSK3β-inhibitor, Chiron, was used for β-catenin stabilization and Wnt pathway induction. PrE cells from two patients (AA8, AA9) and the benign 957E cell line grown with 1,25D had decreased nuclear β-catenin after Chiron treatment compared with vehicle controls (Figure 3C). Consistent with reduced β-catenin activity, 1,25D abrogated Chiron-induced activation of the Wnt response gene *AXIN2* (Figure 3D). Knockdown of VDR in AA1 monolayer cells (Figures 3E and S8A–S8C) blocked 1,25D's ability to inhibit *AXIN2* after Chiron treatment (Figure 3E). Overall, these data support an inhibitory effect of 1,25D on the canonical Wnt pathway and implicate direct regulation via VDR.

1,25D inhibits Dickkopf family member 3

Dickkopf family member 3 (*DKK3*) emerged as a 1,25D target in both the scRNAseq dataset and the RT-qPCR array, so its expression was profiled in a panel of prostate cell lines, monolayer PrE cells, and organoids (Figure 4A). All the cell lines, both immortalized benign (RWPE1 and 957E) and PCa (LAPC4 and PC3), had very low or undetectable *DKK3* expression. DKK3 is also known as "Reduced Expression in Immortalized Cells" (Hsieh et al., 2004), thus our findings are consistent with previous reports of limited expression in cell lines. Across PrE cells grown as monolayers or organoids, 1,25D inhibited *DKK3* expression (Figure 4A).

Immunofluorescence for DKK3 revealed a vesicular and perinuclear staining pattern (Figure 4B, white box), similar to other secreted members of the Dickkopf family (Glinka et al., 1998; Inoue et al., 2017). ELISA showed that culture in 1,25D reduced DKK3 secretion in media (Figure 4C), and western blots of cell lysates showed reduced intracellular protein levels with 1,25D treatment (Figure 4D). Western blot of DKK3 detected several sized bands, agreeing with preceding reports describing many variants: a heavy secreted-form (sDKK3), a lighter intracellular variant (DKK3b), and a 50-kDa secreted form (sDKK3) (Abarzua et al., 2005; Hsieh et al., 2004; Kawano et al., 2006; Leonard et al., 2017; Zenzmaier et al., 2008; Zhang et al., 2010). The 957E cell line had no detectable expression of sDKK3 and faint expression of DKK3b, uniform with the low RNA expression observed. PrE cells grown as monolayers and organoids showed reductions in all variants of DKK3 with sufficient 1,25D compared with controls (Figure 4D). Analysis of our previously published VDR-ChIP-seq dataset (Baumann et al., 2019) in PrE cells showed a peak 20 kb upstream of DKK3 after 1,25D treatment (Figure 4E), supporting potential genomic regulation by VDR.

To emulate 1,25D actions, PrE cells were transduced with lentivirus containing an siDKK3 sequence and GFP tag and grown as organoids in the presence of vehicle or 10 nM 1,25D (Figure 4F, left). Knockdown alone did not recapitulate the effect of 1,25D treatment, but combination of siDKK3 with 1,25D significantly enhanced the effect of vitamin D on organoid area (Figure 4F, right). To rescue 1,25D inhibition of DKK3, exogenous recombinant DKK3 (rDKK3) was added to culture. Treatment with rDKK3 enhanced all DKK3 variants within cell lysates (Figure 4F, left). PrE organoids from three patients were grown in media supplemented with vehicle, 1,25D, or 1,25D in combination with 50 ng/mL rDKK3 for 2 weeks. rDKK3 did not affect organoid area under vehicle conditions, but blocked the increase in area seen in 1,25D-treated organoids (Figure 4G). In sum, these data support that inhibition of DKK3 by 1,25D serves to promote organoid growth.

1,25D suppresses DKK3

The function of DKK3 in the Wnt pathway is not well understood, but it has been shown to inhibit proliferation in prostate and breast cancer cell lines (Leonard et al., 2017). Expression of *DKK3* and *KRT13* was mutually exclusive in the scRNAseq dataset, suggesting that *DKK3* is expressed only in lineage-committed cells (Figure 5A, lower). To observe lineage-committed cells and separate them from progenitor and stem cells, the scRNAseq data was subset into three groups based on *KRT13* expression (Figure 5B, left). *DKK3* was expressed at both time points and most visibly inhibited by 1,25D at day 14 (Figure 5B, right), indicating stronger inhibition with increased length of exposure. Immunofluorescence for CK13 and DKK3 in organoids showed no co-localization (Figure 5C). To observe expression across organoid differentiation trajectories, day 8 and day 14 vehicle scRNAseq datasets were plotted together in pseudotime using

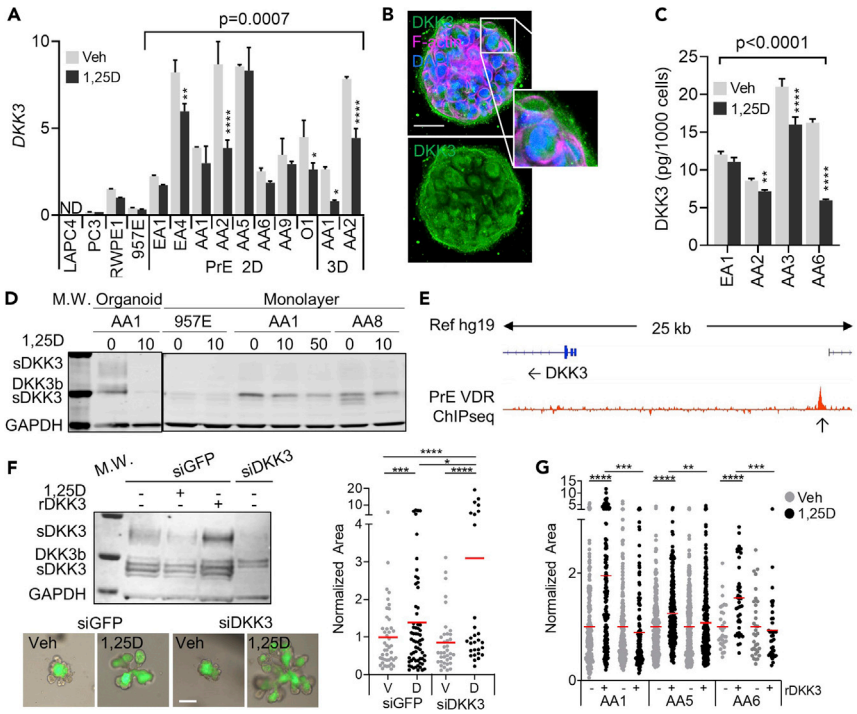

Figure 4. 1,25D inhibits Dickkopf family member 3 (DKK3)

(A) RT-qPCR of *DKK3* expression in prostate cell lines (LAPC4, PC3, RWPE1, 957E), monolayer prostate epithelial cells (PrE 2D), and organoid PrE cells (3D) grown in vehicle or 10 nM 1,25D. Monolayer cells were treated for 24–72 h, and organoids were treated for 2–3.5 weeks. Relative quantitation is normalized to *HPRT1*; error bars represent standard deviation of technical RT-qPCR pipetting replicates. Cells from multiple sources represent biological replicates. p value represents interaction outcome of grouped two-way ANOVA comparison of vehicle versus 1,25D in PrE cells using different patients as biological replicates; individual p values are shown (*$p < 0.1$; **$p < 0.05$; ****$p < 0.001$).

(B) Immunostaining for DKK3 (green) in a whole-mounted day 17 AA3 organoid counterstained with DAPI (blue) and phalloidin/F-actin (pink). Scale bar, 50 μm.

(C) ELISA quantification of secreted DKK3 in media collected from monolayer PrE cells grown in vehicle or 10 nM 1,25D for 72 h, normalized to the number of cells. Error bars represent the standard error of triplicate ELISA technical samples. Cells from multiple sources present biological replicates. p value represents interaction outcome of grouped two-way ANOVA comparison of vehicle versus 1,25D using different patients as biological replicates, individual p values are shown (**$p < 0.05$; ****$p < 0.001$).

(D) Western blot of DKK3 expression in cell lines and in monolayer and organoid PrE cells grown in vehicle or 10 nM 1,25D (sDKK3, secreted DKK3 variants; DKK3b, intracellular DKK3 variant); molecular weight marker shown (M.W.).

(E) VDR-ChIP sequencing peak near DKK3 in PrE cells treated with 1,25D for 3 h; IGV track showing 1,25D-treated minus vehicle-treated coverage (data from NCBI GEO accession number GSE124576).

(F) Western blot of monolayer AA1 prostate epithelial (PrE) cells transduced with control virus (siGFP) or siDKK3 virus and grown in vehicle, 10 nM 1,25D, or 50 ng/mL rDKK3 (upper left); molecular weight marker shown (M.W.). Representative images of siGFP- or siDKK3-treated AA1 PrE organoids grown in vehicle or 10 nM 1,25D for 2 weeks (lower left), with quantification of relative area (right). Area was normalized to the mean of the vehicle, showing ≥3 replicate wells for each condition; each dot represents an organoid. (*$p < 0.1$;***$p < 0.01$; ****$p < 0.001$. Scale bar, 200 μm).

(G) Relative area of PrE organoids grown in vehicle or 10 nM 1,25D combined with 50 ng/mL rDKK3 treatment for 2 weeks. Area was normalized to the mean of the vehicle, showing ≥3 replicate wells for each condition, each dot represents an organoid. (**$p < 0.05$; ***$p < 0.01$; ****$p < 0.001$).

Monocle 3 (Figure 5D). *KRT13* was expressed at the beginning of pseudotime, with cells from day 8 and day 14 samples found at this stage, showing the resident stem cells in organoid culture (Hu et al., 2017). Day 8 cells clustered halfway through the differentiation trajectory where *MKI67* expression is high, and day 14 cells clustered at the end. A fork was seen in day 14 cells, possibly where basal and luminal lineages start to diverge. *DKK3* expression increased across pseudotime, consistent with expression in lineage-committed cells and indicating its upregulation in senescence (Untergasser et al., 2002) (Figure 5D, bottom right).

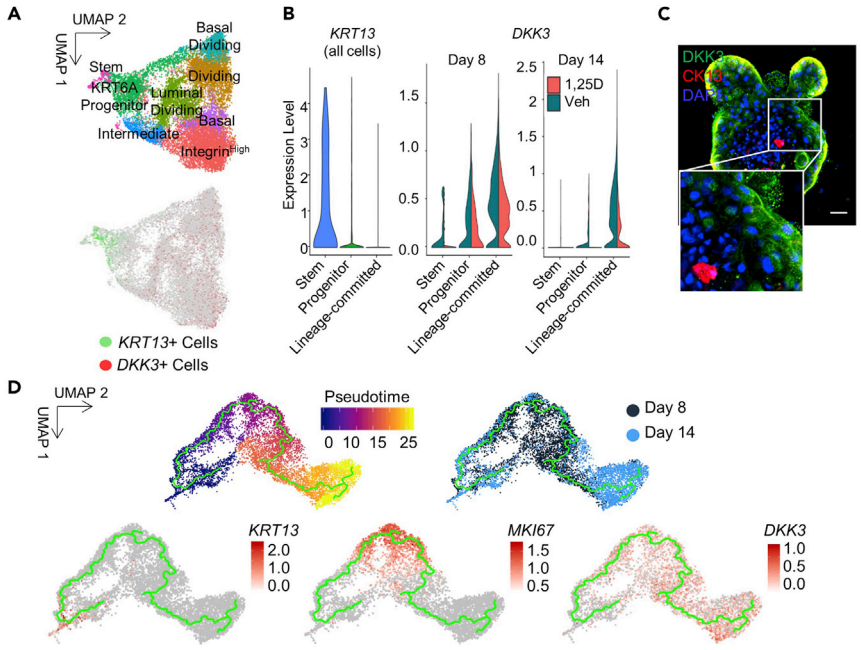

Figure 5. 1,25D suppresses DKK3

(A) UMAP of integrated scRNAseq dataset shown in Figure 2A (upper); blended UMAP of integrated scRNAseq data showing expression of *KRT13* (green) and *DKK3* (red) (lower).

(B) Violin plot of integrated dataset shown in (A), subset by *KRT13* expression into lineage-committed, progenitor, or stem populations (left). Violin plots of integrated dataset shown in (A), separated by time point, showing *DKK3* expression (right) in vitamin D (pink) and vehicle (teal) samples.

(C) DKK3 (green) and CK13 (red) expression in whole-mounted AA3 organoid counterstained with DAPI (blue). Scale bar, 50 μm.

(D) Pseudotime of integrated scRNAseq data for day 8 and day 14 vehicle samples (upper left). Sample distribution across pseudotime for day 8 (dark blue) and day 14 (light blue) cells (upper right). *KRT13* (lower left), *MKI67* (lower middle), and *DKK3* (lower right) expression across pseudotime.

Vitamin D regulates the Wnt pathway and DKK3 in prostate tissue slice explants

To determine if the Wnt pathway and DKK3 are targets of vitamin D *in situ*, fresh benign prostate tissue slices from a patient undergoing radical prostatectomy were cultured *ex vivo* for 8 h in vehicle and vitamin D using precision-cut fresh tissue sections (Maund et al., 2014). Gene expression was determined by spatial transcriptomics with RNA sequencing (Stahl et al., 2016). DKK3 was expressed in both prostate stroma and epithelium (Figure 6A), compared with the epithelial marker NKX3.1 and stromal marker FGF7 (Figure 6A). Due to spot size of 55 μm, the resolution of spatial transcriptomics is not at the single-cell level, so the captured areas are not completely pure for one distinct cell type (Stahl et al., 2016). As such, spots enriched in pooled epithelial markers were selected to compare deficient (veh) and sufficient vitamin D conditions in prostate epithelium.

The expression of genes known to be upregulated by Wnt signaling was queried in the spatial dataset (Figure 6B). The 19 genes are per the curated list from Roel Nusse Lab at Stanford University (Nusse, 2020), selecting only genes that are direct Wnt targets. More than half of the genes were downregulated with vitamin D, suggesting a net suppression of Wnt activity. Specifically, *FST*, *MYC*, *MMP7*, *TCF4*, and *JUN* were significantly lower. *AXIN2* was not significantly decreased, but it had an extremely low base level of detection, which hindered its analysis. Similarly, whereas *DKK3* was markedly lower in the vitamin D-sufficient tissue (Figure 6C), the means did not achieve a significant difference due to the limited number of spots captured in the vitamin D sample. Together these findings are consistent with *in vitro* data and support the regulation of Wnt activity and DKK3 by vitamin D in intact prostate tissue

Discussion

The prostate is a hormonally regulated gland that requires steroids for development, and dysregulation of hormones occurs during carcinogenesis and late-stage PCa. Vitamin D is a steroid hormone that promotes

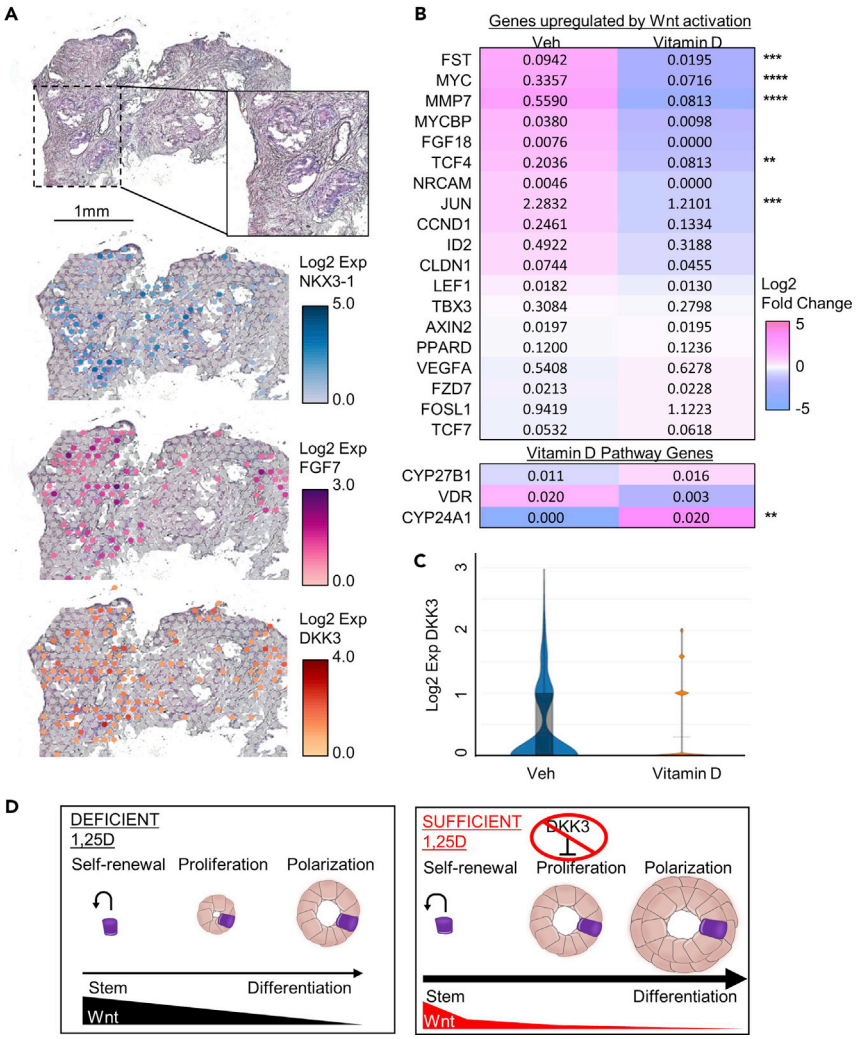

Figure 6. Vitamin D inhibits DKK3 in prostate tissue slice explants by spatial transcriptional profiling

(A) H&E of vehicle-treated tissue slice with spatial mapping of mRNAs for *DKK3* (red), *NKX3.1* (epithelial marker, blue), and *FGF7* (stromal marker, magenta). Gene expression determined by 10X Visium spatial profiling and shown as log2 relative expression.

(B) Heatmap depicting expression of genes upregulated by Wnt pathway activation (Nusse, 2020) and the vitamin D pathway in epithelium of prostate tissue slices cultured in vehicle control (veh) or 25D (vitamin D) (Nusse, 2020). Color scale shows log2 fold change; number inset shows average expression calculated by Loupe software. p values are adjusted using the Benjamini-Hochberg correction for multiple tests, ****$p < 0.001$, ***$p < 0.01$, ** $p < 0.05$.

(C) Violin plot of the average log2 counts for DKK3 in control and 25D (vitamin D)-treated epithelium. Horizontal bar = mean, box = 95% confidence interval.

(D) Diagram summarizing the effects of 1,25D on prostate epithelial organoids. Under vehicle conditions "DEFICIENT 1,25D," a self-renewing stem cell with high Wnt activity undergoes asymmetric division to produce progenitor cells that will rapidly expand. As differentiation occurs, downstream cells will have reduced Wnt activity. Under sufficient conditions, "SUFFICIENT 1.25D," proliferation is enhanced through inhibition of DKK3, resulting in a larger organoid. Wnt signaling is also inhibited in lineage-committed cells through β-catenin sequestration, to promote differentiation away from a stem cell phenotype.

differentiation in many cell types, yet its role has not been studied in the differentiation of benign human prostate epithelium. Using primary epithelial organoids from multiple patients, we found that continuous culture in physiologically relevant concentrations of 1,25D promoted differentiation and increased organoid area compared with vitamin D-deficient conditions (Figures 1 and 2). The dominant mechanisms were inhibition of the canonical Wnt pathway (Figures 3 and 6) and reduction of Wnt pathway member DKK3 (Figures 4, 5, and 6), to promote epithelial growth (Figure 6D). These findings were corroborated

in fresh patient tissue explants in which vitamin D also reduced Wnt target gene expression and DKK3 (Figure 6).

The Wnt pathway is known to be highly active in prostate stem cells compared with differentiated cells (Blum et al., 2009). In kidney organoids and prostate organogenesis, Wnt activity is critical early on to promote progenitor outgrowth but then decreases to allow for differentiation (Prins and Putz, 2008; Simons et al., 2012; Takasato et al., 2016). Similarly, in snake venom gland organoids, Wnt agonists must be removed to allow for differentiation and secretory function (Post et al., 2020). Consistently, we observed that lineage-committed cells had lower Wnt activity and selective Wnt inhibition by 1,25D was observed in the lineage-committed cells, but not in *KRT13+* stem cells, resulting in enhanced epithelial differentiation in the organoids (Figure 6D). This effect of vitamin D complements the reports of Wnt pathway regulation in other epithelial models. Kovalenko et al. reported that 1,25D inhibited Wnt and promoted genes that are "induced during differentiation" from Gene Set Analysis in the benign prostate RWPE1 cell line (Kovalenko et al., 2010). In colon cancer cell lines and mouse colon tissue, 1,25D inhibited the Wnt pathway by decreased nuclear β-catenin and increased cellular differentiation (Aguilera et al., 2007; Groschel et al., 2016; Larriba et al., 2013). Similar results of β-catenin by vitamin D metabolites were observed in Kaposi sarcoma (Tapia et al., 2020) and renal cell carcinoma (Xu et al., 2020).

In PCa, Wnt signaling has been shown to promote resistance to androgen deprivation therapy (Yokoyama et al., 2014). PCa stem cells show increased nuclear β-catenin, and TCF/LEF activity (Zhang et al., 2017) and Lef-1 identifies an androgen-insensitive population of basal progenitors in mouse prostate maturation (Wu et al., 2011). As PCa progresses, *APC* and *CTNNB1* become mutated in 22% castration-resistant PCa to drive Wnt pathway activation (Murillo-Garzon and Kypta, 2017). In PCa cell lines, disruption of e-cadherin enhanced Wnt signaling and increased tumor growth (Davies et al., 2000) and WNT5A has been shown to promote cancer cell invasion (Wang et al., 2020). Our results indicate that vitamin D sufficiency could provide negative pressure on the Wnt pathway to complement other therapies and improve PCa patient outcome.

DKK3 emerged as potently and consistently inhibited by 1,25D in the prostate organoids and monolayer cells. Our findings suggest an anti-proliferative role for DKK3 in prostate organoids, and this adds to the literature that is unclear about the downstream target of this protein in prostate cells. In general, the Dickkopf family members are inhibitors of Wnt signaling, such as DKK1 (Glinka et al., 1998; Kruithof-De Julio et al., 2013). However, DKK3 is the most structurally divergent member of the Dickkopf family (Krupnik et al., 1999) and has varied effects on Wnt, ranging from no effect (Krupnik et al., 1999; Pinho Christof Niehrs, 2007; Romero et al., 2013) to promoting (Ferrari et al., 2019; Nakamura and Hackam, 2010; Yin et al., 2018) or inhibiting Wnt activity (Bhattacharyya et al., 2017; Leonard et al., 2017; Liu et al., 2019; Sharma Das et al., 2013). DKK3 also functions as both a positive and negative regulator of TGFβ signaling, depending on the model (Al Shareef et al., 2018; Busceti et al., 2017; Kardooni et al., 2018; Li et al., 2017; Pinho Christof Niehrs, 2007; Romero et al., 2013; Wang et al., 2015b), but DKK3 did not impact TGFβ in this study (data not shown). Despite possibly conflicting reports of DKK3's signaling targets, it has consistently been shown to restrain cell proliferation (Kawano et al., 2006; Leonard et al., 2017). It acts as a cell cycle inhibitor whose expression is reduced in immortalized cells (Kawano et al., 2006), upregulated in senescent PrE cells at passage 10 compared with passage 3 (Untergasser et al., 2002) and upregulated during aging (Yin et al., 2018). In developing mouse prostate, addition of exogenous DKK3 blunted proliferation, preventing luminal differentiation, Nkx3.1 expression, and epithelial bud formation (Kruithof-De Julio et al., 2013). Our findings that 1,25D reduction of DKK3 resulted in increased organoid size is similar to the DKK3-deficient mice, which are viable with normal prostate glands, but have increased Ki-67+ proliferating cells (Romero et al., 2013). We observed that DKK3 was not expressed by the stem cells in organoids, similar to patient tissue (Henry et al., 2018), indicating that DKK3 acts downstream to regulate cell growth (Figure 6D). Notably, DKK3 is reported highly expressed in the stroma of the prostate, which indicates a multifaceted role for this protein that can be explored in the future using co-culture models (Al Shareef et al., 2018; Henry et al., 2018; Zenzmaier et al., 2013). The increase in organoid size induced by 1,25D may seem contradictory to the traditional anti-proliferative role of vitamin D metabolites (Feldman et al., 2014; Murphy et al., 2017; Wagner et al., 2013). However, the organoid model was optimized to create a permissive environment for expansion and differentiation of stem/progenitor cells and is supplemented with androgen to drive cell division.

In summary, we report two complementary mechanisms by which vitamin D sufficiency promotes prostate epithelial differentiation—inhibition of canonical Wnt signaling and the protein DKK3. This is the first

report, to our knowledge, of the hormone vitamin D regulating DKK3 expression in the prostate. These findings are particularly impactful for patients who are frequently deficient in vitamin D, such as African Americans and adults older than 70 years, who have significantly high rates of PCa (Jacques et al., 1997; Murphy et al., 2014).

Limitations of the study

Access to primary cells from multiple, ancestrally diverse patients; fresh tissue explants; and the use of scRNAseq and spatial transcriptomics are the major strengths of this study, yet they are not without limitations. Patient-derived cells have inherent inter-patient heterogeneity and epithelial content in the tissue collected; as a result the aliquots available differ between patients. To address this, we used as many patients as possible for each endpoint and supplemented with cell lines if necessary. scRNAseq and spatial transcriptomics are powerful tools to analyze the transcriptomes of thousands of cells from heterogenous samples, but it only captures a subset of the transcripts in each cell (~30%–32% of transcripts for the 10x Chromium Single cell v3 kit). Thus, the lack of a transcript does not mean that protein is absent; for example, *DPP4* and *AR* were low in the scRNAseq data, but CD26 was detected by flow cytometry, nuclear AR was detected by IHC, and $CK8^{+}/p63^{-}$ cells were observed (Figures 1E and 2D). As well, because the organoids were completely epithelial without other cell types, the data lack extremely different clusters. However, our clusters were transcriptionally distinct and similar to those observed in scRNAseq data from the epithelial clustering of whole patient prostate tissue (Henry et al., 2018). When assigning cluster markers and interpreting scRNAseq data, the use of the terms "lineage-committed" and "stem" were guided by previously reported findings established in the literature. Our experiments did not utilize flow cytometry to isolate stem cells and demonstrate that organoids initiated exclusively from CK13/PRAC1 populations. Because of this, organoids may have initiated from cells at various points along the stem and progenitor hierarchy, although it is widely believed that terminally differentiated epithelial cells are unable to form organoids in culture. These assumptions do not impact the conclusions that vitamin D inhibits canonical Wnt activity and DKK3 in prostate epithelial cells, but caution should be used when interpreting terms "lineage-committed" and "stem." Despite these limitations, the approach successfully identified vitamin D-regulated genes and pathways that were validated by multiple assays.

Resource availability

Lead contact

Lead Contact, Larisa Nonn (lnonn@uic.edu).

Materials availability

Further information and requests for resources and reagents should be directed to and will be fulfilled by the Lead Contact, Larisa Nonn (lnonn@uic.edu). This study did not generate new unique reagents.

Data and code availability

ScRNAseq data has been submitted to NCBI Gene Expression Omnibus and can be found under accession number GSE142489. ChIP sequencing data can be found under accession number GSE124576. Spatial transcriptomics data can be found under accession number GSE159697.

Methods

All methods can be found in the accompanying Transparent methods supplemental file.

Supplemental information

Supplemental Information can be found online at https://doi.org/10.1016/j.isci.2020.101974.

Acknowledgments

We thank UIC Biorepository (Alex Susma), and urologists (Drs. Daniel Moreira, and Simone Crivallero) for facilitation of tissue acquisition for patient-derived cultures. We thank UIC Urology patients for donating their tissue—without their participation, none of this research would be possible. We thank Dr. Ke Ma with UIC Fluorescence Imaging Core for assistance with confocal. We thank Dr. Matt McDougall of the Merrill laboratory for his counsel with the Wnt pathway. We thank Dr. Alvaro Hernandez, Chris Wright, Jenny Zadeh, and Jessica Holmes and the UIUC DNA services team for sequencing support and the CellRanger

pipeline. We thank Magdalena Rogozinska and Dr. Gayatry Mohapatra for their help with TapeStation quantification. We thank UIC Pathology Department members Joseph Marsili, Morgan Zenner, Dr. Larischa DeWet, and Lenny Hong for their thoughts and troubleshooting. We thank Junbin Huang for his participation on the project through ResearcHStart. Graphical abstract was created with www.BioRender.com. This work was funded, in part, by the Department of Defense Prostate Cancer Research Program Health Disparities Idea Award PC121923 (Nonn) and the UIC Center for Clinical and Translation Science Pre-Doctoral Education for Clinical and Translational Scientists (PECTS) Program (McCray). The content is solely the responsibility of the authors and does not necessarily represent the official views of the National Institutes of Health or Department of Defense.

Author contributions

Conceptualization, T.M. and L.N.; Formal analysis, T.M.; Investigation, T.M., J.P., C.L., J.G., B.B., and M.J.S.; Resources, L.N., K.V.-N., and M.R.A.; Writing, T.M., B.B., and L.N.; Visualization, T.M.; Supervision, L.N.; Funding acquisition, L.N.

Declaration of interests

The authors declare no competing interests.

Received: May 1, 2020
Revised: August 11, 2020
Accepted: December 17, 2020
Published: January 22, 2021

References

Abarzua, F., Sakaguchi, M., Takaishi, M., Nasu, Y., Kurose, K., Ebara, S., Miyazaki, M., Namba, M., Kumon, H., and Huh, N.-h. (2005). Adenovirus-mediated overexpression of REIC/Dkk-3 selectively induces apoptosis in human prostate cancer cells through activation of c-Jun-NH2-kinase. Cancer Res. *65*, 9617–9622.

Abe, E., Miyaura, C., Sakagami, H., Takeda, M., Konno, K., Yamazaki, T., Yoshiki, S., and Suda, T. (1981). Differentiation of mouse myeloid leukemia cells induced by 1 alpha,25-dihydroxyvitamin D3. Proc. Natl. Acad. Sci. U S A *78*, 4990–4994.

Aguilera, O., Pena, C., Garcia, J.M., Larriba, M.J., Ordonez-Moran, P., Navarro, D., Barbachano, A., Lopez de Silanes, I., Ballestar, E., Fraga, M.F., et al. (2007). The Wnt antagonist DICKKOPF-1 gene is induced by 1alpha,25-dihydroxyvitamin D3 associated to the differentiation of human colon cancer cells. Carcinogenesis *28*, 1877–1884.

Al Shareef, Z., Kardooni, H., Murillo-Garzón, V., Domenici, G., Stylianakis, E., Steel, J.H., Rabano, M., Gorroño-Etxebarria, I., Zabalza, I., dM Vivanco, M., et al. (2018). Protective effect of stromal Dickkopf-3 in prostate cancer: opposing roles for TGFBI and ECM-1. Oncogene *37*, 5305–5324.

Banks, M., and Holick, M.F. (2015). Molecular mechanism(s) involved in 25-Hydroxyvitamin D's antiproliferative effects in CYP27B1-transfected LNCaP cells. Anticancer Res. *35*, 3773–3779.

Barros-Silva, J.D., Linn, D.E., Steiner, I., Guo, G., Ali, A., Pakula, H., Ashton, G., Peset, I., Brown, M., Clarke, N.W., et al. (2018). Single-Cell analysis identifies LY6D as a marker linking castration-resistant prostate luminal cells to prostate progenitors and cancer. Cell Rep. *25*, 3504–3518.

Baumann, B., Lugli, G., Gao, S., Zenner, M., and Nonn, L. (2019). High levels of PIWI-interacting RNAs are present in the small RNA landscape of prostate epithelium from vitamin D clinical trial specimens. Prostate *79*, 840–855.

Bhattacharyya, S., Feferman, L., Tobacman, J.K., Bhattacharyya, S., Feferman, L., and Tobacman, J.K. (2017). Chondroitin sulfatases differentially regulate Wnt signaling in prostate stem cells through effects on SHP2, phospho-ERK1/2, and Dickkopf Wnt signaling pathway inhibitor (DKK3). Oncotarget *8*, 100242–100260.

Bikle, D.D. (2004). Vitamin D regulated keratinocyte differentiation. J. Cell. Biochem. *92*, 436–444.

Blum, R., Gupta, R., Burger, P.E., Ontiveros, C.S., Salm, S.N., Xiong, X., Kamb, A., Wesche, H., Marshall, L., Cutler, G., et al. (2009). Molecular signatures of prostate stem cells reveal novel signaling pathways and provide insights into prostate cancer. PLoS One *4*, e5722.

Bouillon, R., Carmeliet, G., Verlinden, L., van Etten, E., Verstuyf, A., Luderer, H.F., Lieben, L., Mathieu, C., and Demay, M. (2008). Vitamin D and human health: lessons from vitamin D receptor null mice. Endocr. Rev. *29*, 726–776.

Bryant, S.L., Francis, J.C., Lokody, I.B., Wang, H., Risbridger, G.P., Loveland, K.L., and Swain, A. (2014). Sex specific retinoic acid signaling is required for the initiation of urogenital sinus bud development. Dev. Biol. *395*, 209–217.

Busceti, C.L., Marchitti, S., Bianchi, F., Di Pietro, P., Riozzi, B., Stanzione, R., Cannella, M., Battaglia, G., Bruno, V., Volpe, M., et al. (2017). Dickkopf-3 upregulates VEGF in cultured human endothelial cells by activating activin receptor-like kinase 1 (ALK1) pathway. Front. Pharmacol. *8*, 111.

Butler, A., Hoffman, P., Smibert, P., Papalexi, E., and Satija, R. (2018). Integrating single-cell transcriptomic data across different conditions, technologies, and species. Nat. Biotech. *36*, 411.

Campbell, M.J., Elstner, E., Holden, S., Uskokovic, M., and Koeffler, H.P. (1997). Inhibition of proliferation of prostate cancer cells by a 19-nor-hexafluoride vitamin D3 analogue involves the induction of p21waf1, p27kip1 and E-cadherin. J. Mol. Endocrinol. *19*, 15–27.

Chandler, P.D., Giovannucci, E.L., Scott, J.B., Bennett, G.G., Ng, K., Chan, A.T., Hollis, B.W., Emmons, K.M., Fuchs, C.S., and Drake, B.F. (2014). Null association between vitamin D and PSA levels among black men in a vitamin D supplementation trial. Cancer Epidemiol. Biomarkers Prev. *23*, 1944–1947.

Chen, K.S., and DeLuca, H.F. (1995). Cloning of the human 1 alpha,25-dihydroxyvitamin D-3 24-hydroxylase gene promoter and identification of two vitamin D-responsive elements. Biochim. Biophys. Acta *1263*, 1–9.

Davies, G., Jiang, W.G., and Mason, M.D. (2000). Cell-cell adhesion molecules and signaling intermediates and their role in the invasive potential of prostate cancer cells. J. Urol. *163*, 985–992.

Drost, J., Karthaus, W.R., Gao, D., Driehuis, E., Sawyers, C.L., Chen, Y., and Clevers, H. (2016). Organoid culture systems for prostate epithelial and cancer tissue. Nat. Protoc. *11*, 347–358.

Elshazly, M.A., Sultan, M.F., Aboutaleb, H.A., Salem, S.M., Aziz, M.S., Abd Elbaky, T.M., Elsherif, E.A., Gawish, M.M., Alajrawi, F.T., Elgadi, F.A.A.,

et al. (2017). Vitamin D deficiency and lower urinary tract symptoms in males above 50 years of age. Urol. Ann. *9*, 170–173.

Fang, F., Kasperzyk, J.L., Shui, I., Hendrickson, W., Hollis, B.W., Fall, K., Ma, J., Gaziano, J.M., Stampfer, M.J., Mucci, L.A., et al. (2011). Prediagnostic plasma vitamin D metabolites and mortality among patients with prostate cancer. PLoS One *6*, e18625.

Feldman, D., Krishnan, A.V., Swami, S., Giovannucci, E., and Feldman, B.J. (2014). The role of vitamin D in reducing cancer risk and progression. Nat. Rev. Cancer *14*, 342–357.

Ferrari, N., Ranftl, R., Chicherova, I., Slaven, N.D., Moeendarbary, E., Farrugia, A.J., Lam, M., Semiannikova, M., Westergaard, M.C.W., Tchou, J., et al. (2019). Dickkopf-3 links HSF1 and YAP/TAZ signalling to control aggressive behaviours in cancer-associated fibroblasts. Nat. Commun. *10*, 130.

Fleet, J.C., Kovalenko, P.L., Li, Y., Smolinski, J., Spees, C., Yu, J.G., Thomas-Ahner, J.M., Cui, M., Neme, A., Carlberg, C., et al. (2019). Vitamin D signaling suppresses early prostate carcinogenesis in TgAPT121 mice. Cancer Prev. Res. (Phila) *12*, 343–356.

Genevet, A., and Tapon, N. (2011). The Hippo pathway and apico-basal cell polarity. Biochem. J. *436*, 213–224.

Gilbert, R., Metcalfe, C., Oliver, S.E., Whiteman, D.C., Bain, C., Ness, A., Donovan, J., Hamdy, F., Neal, D.E., Lane, J.A., et al. (2009). Life course sun exposure and risk of prostate cancer: population-based nested case-control study and meta-analysis. Int. J. Cancer *125*, 1414–1423.

Giovannucci, E., Liu, Y., Rimm, E.B., Hollis, B.W., Fuchs, C.S., Stampfer, M.J., and Willett, W.C. (2006). Prospective study of predictors of vitamin D status and cancer incidence and mortality in men. J. Natl. Cancer Inst. *98*, 451–459.

Glinka, A., Wu, W., Delius, H., Monaghan, A.P., Blumenstock, C., and Niehrs, C. (1998). Dickkopf-1 is a member of a new family of secreted proteins and functions in head induction. Nature *391*, 357–362.

Goldstein, A.S., Lawson, D.A., Cheng, D., Sun, W., Garraway, I.P., and Witte, O.N. (2008). Trop2 identifies a subpopulation of murine and human prostate basal cells with stem cell characteristics. Proc. Natl. Acad. Sci. U S A *105*, 20882–20887.

Groschel, C., Aggarwal, A., Tennakoon, S., Hobaus, J., Prinz-Wohlgenannt, M., Marian, B., Heffeter, P., Berger, W., and Kallay, E. (2016). Effect of 1,25-dihydroxyvitamin D3 on the Wnt pathway in non-malignant colonic cells. J. Steroid Biochem. Mol. Biol. *155*, 224–230.

Guo, C., Liu, H., Zhang, B.H., Cadaneanu, R.M., Mayle, A.M., and Garraway, I.P. (2012). Epcam, cd44, and cd49f distinguish sphere-forming human prostate basal cells from a subpopulation with predominant tubule initiation capability. PLoS One *7*, e34219.

Hanchette, C.L., and Schwartz, G.G. (1992). Geographic patterns of prostate cancer mortality. Evidence for a protective effect of ultraviolet radiation. Cancer *70*, 2861–2869.

Hendrickson, W.K., Flavin, R., Kasperzyk, J.L., Fiorentino, M., Fang, F., Lis, R., Fiore, C., Penney, K.L., Ma, J., Kantoff, P.W., et al. (2011). Vitamin D receptor protein expression in tumor tissue and prostate cancer progression. J. Clin. Oncol. *29*, 2378–2385.

Henry, G.H., Malewska, A., Joseph, D.B., Malladi, V.S., Lee, J., Torrealba, J., Mauck, R.J., Gahan, J.C., Raj, G.V., Roehrborn, C.G., et al. (2018). A cellular anatomy of the normal adult human prostate and prostatic urethra. Cell Rep. *25*, 3530–3542.

Hlaing, S.M., Garcia, L.A., Contreras, J.R., Norris, K.C., Ferrini, M.G., and Artaza, J.N. (2014). 1,25-Vitamin D3 promotes cardiac differentiation through modulation of the WNT signaling pathway. J. Mol. Endocrinol. *53*, 303–317.

Holick, C.N., Stanford, J.L., Kwon, E.M., Ostrander, E.A., Nejentsev, S., and Peters, U. (2007). Comprehensive association analysis of the vitamin D pathway genes, VDR, CYP27B1, and CYP24A1, in prostate cancer. Cancer Epidemiol. Biomarkers Prev. *16*, 1990–1999.

Hsieh, S.-Y., Hsieh, P.-S., Chiu, C.-T., and Chen, W.-Y. (2004). Dickkopf-3/REIC functions as a suppressor gene of tumor growth. Oncogene *23*, 9183–9189.

Hu, W.-Y., Hu, D.-P., Xie, L., Li, Y., Majumdar, S., Nonn, L., Hu, H., Shioda, T., and Prins, G.S. (2017). Isolation and functional interrogation of adult human prostate epithelial stem cells at single cell resolution. Stem Cell Res. *23*, 1–12.

Hutabarat, M., Wibowo, N., Obermayer-Pietsch, B., and Huppertz, B. (2018). Impact of vitamin D and vitamin D receptor on the trophoblast survival capacity in preeclampsia. PLoS One *13*, e0206725.

Inoue, J., Fujita, H., Bando, T., Kondo, Y., Kumon, H., and Ohuchi, H. (2017). Expression analysis of Dickkopf-related protein 3 (Dkk3) suggests its pleiotropic roles for a secretory glycoprotein in adult mouse. J. Mol. Histol. *48*, 29–39.

Jacques, P.F., Felson, D.T., Tucker, K.L., Mahnken, B., Wilson, P.W., Rosenberg, I.H., and Rush, D. (1997). Plasma 25-hydroxyvitamin D and its determinants in an elderly population sample. Am. J. Clin. Nutr. *66*, 929–936.

James, S.Y., Williams, M.A., Kelsey, S.M., Newland, A.C., and Colston, K.W. (1997). Interaction of vitamin D derivatives and granulocyte-macrophage colony-stimulating factor in leukaemic cell differentiation. Leukemia *11*, 1017–1025.

Karantanos, T., Corn, P.G., and Thompson, T.C. (2013). Prostate cancer progression after androgen deprivation therapy: mechanisms of castrate resistance and novel therapeutic approaches. Oncogene *32*, 5501–5511.

Kardooni, H., Gonzalez-Gualda, E., Stylianakis, E., Saffaran, S., Waxman, J., and Kypta, R.M. (2018). CRISPR-mediated reactivation of DKK3 expression attenuates TGF-β signaling in prostate cancer. Cancers *10*, 1–19.

Kawano, Y., Kitaoka, M., Hamada, Y., Walker, M., Waxman, J., and Kypta, R. (2006). Regulation of prostate cell growth and morphogenesis by Dickkopf-3. Oncogene *25*, 6528–6537.

Konety, B.R., Schwartz, G.G., Acierno, J.S., Jr., Becich, M.J., and Getzenberg, R.H. (1996). The role of vitamin D in normal prostate growth and differentiation. Cell Growth Differ. *7*, 1563–1570.

Kovalenko, P.L., Zhang, Z., Cui, M., Clinton, S.K., and Fleet, J.C. (2010). 1,25 dihydroxyvitamin D-mediated orchestration of anticancer, transcript-level effects in the immortalized, non-transformed prostate epithelial cell line, RWPE1. BMC Genomics *11*, 26.

Kramer, A., Green, J., Pollard, J., Jr., and Tugendreich, S. (2014). Causal analysis approaches in ingenuity pathway analysis. Bioinformatics *30*, 523–530.

Kruithof-De Julio, M., Shibata, M., Desai, N., Reynon, M., Halili, M.V., Hu, Y.-P., Price, S.M., Abate-Shen, C., and Shen, M.M. (2013). Canonical Wnt signaling regulates Nkx3.1 expression and luminal epithelial differentiation during prostate organogenesis. Dev. Dyn. *242*, 1160–1171.

Krupnik, V.E., Sharp, J.D., Jiang, C., Robison, K., Chickering, T.W., Amaravadi, L., Brown, D.E., Guyot, D., Mays, G., Leiby, K., et al. (1999). Functional and structural diversity of the human Dickkopf gene family. Gene *238*, 301–313.

Larriba, M.J., González-Sancho, J.M., Barbáchano, A., Niell, N., Ferrer-Mayorga, G., and Muñoz, A. (2013). Vitamin D is a multilevel repressor of Wnt/β-catenin signaling in cancer cells. Cancers (Basel) *5*, 1242–1260.

Larriba, M.J., Ordonez-Moran, P., Chicote, I., Martin-Fernandez, G., Puig, I., Munoz, A., and Palmer, H.G. (2011). Vitamin D receptor deficiency enhances Wnt/beta-catenin signaling and tumor burden in colon cancer. PLoS One *6*, e23524.

Leonard, J.L., Leonard, D.M., Wolfe, S.A., Liu, J., Rivera, J., Yang, M., Leonard, R.T., Johnson, J.P.S., Kumar, P., Liebmann, K.L., et al. (2017). The Dkk3 gene encodes a vital intracellular regulator of cell proliferation. PLoS One *12*, e0181724.

Li, Y., Liu, H., Liang, Y., Peng, P., Ma, X., and Zhang, X. (2017). DKK3 regulates cell proliferation, apoptosis and collagen synthesis in keloid fibroblasts via TGF-β1/Smad signaling pathway. Biomed. Pharmacother. *91*, 174–180.

Liu, B., Zhou, W., Jiang, H., Xiang, Z., and Wang, L. (2019). miR-1303 promotes the proliferation, migration and invasion of prostate cancer cells through regulating the Wnt/beta-catenin pathway by targeting DKK3. Exp. Ther. Med. *18*, 4747–4757.

MacLaughlin, J.A., Cantley, L.C., and Holick, M.F. (1990). 1,25(OH)2D3 increases calcium and phosphatidylinositol metabolism in differentiating cultured human keratinocytes. J. Nutr. Biochem. *1*, 81–87.

Manson, J.E., Cook, N.R., Lee, I.-M., Christen, W., Bassuk, S.S., Mora, S., Gibson, H., Gordon, D., Copeland, T., D'Agostino, D., et al. (2019). Vitamin D supplements and prevention of cancer and cardiovascular disease. N. Engl. J. Med. *380*, 33–44.

Marshall, D.T., Savage, S.J., Garrett-Mayer, E., Keane, T.E., Hollis, B.W., Horst, R.L., Ambrose, L.H., Kindy, M.S., and Gattoni-Celli, S. (2012). Vitamin D3 supplementation at 4000 international

units per day for one year results in a decrease of positive cores at repeat biopsy in subjects with low-risk prostate cancer under active surveillance. J. Clin. Endocrinol. Metab. *97*, 2315–2324.

Martin, J.L., and Pattison, S.L. (2000). Insulin-like growth factor binding protein-3 is regulated by dihydrotestosterone and stimulates deoxyribonucleic acid synthesis and cell proliferation in LNCaP prostate carcinoma cells. Endocrinology *141*, 2401–2409.

Maund, S.L., Nolley, R., and Peehl, D.M. (2014). Optimization and comprehensive characterization of a faithful tissue culture model of the benign and malignant human prostate. Lab. Invest. *94*, 208–221.

McCray, T., Moline, D., Baumann, B., Vander Griend, D.J., and Nonn, L. (2019). Single-cell RNA-Seq analysis identifies a putative epithelial stem cell population in human primary prostate cells in monolayer and organoid culture conditions. Am. J. Clin. Exp. Urol. *7*, 123–138.

Mucuk, G., Sepet, E., Erguven, M., Ekmekci, O., and Bilir, A. (2017). 1,25-Dihydroxyvitamin D3 stimulates odontoblastic differentiation of human dental pulp-stem cells in vitro. Connect. Tissue Res. *58*, 531–541.

Muralidhar, S., Filia, A., Nsengimana, J., Pozniak, J., O'Shea, S.J., Diaz, J.M., Harland, M., Randerson-Moor, J.A., Reichrath, J., Laye, J.P., et al. (2019). Vitamin D-VDR signaling inhibits Wnt/beta-catenin-mediated melanoma progression and promotes antitumor immunity. Cancer Res. *79*, 5986–5998.

Murillo-Garzon, V., and Kypta, R. (2017). WNT signalling in prostate cancer. Nat. Rev. Urol. *14*, 683–696.

Murphy, A.B., Nyame, Y., Martin, I.K., Catalona, W.J., Hollowell, C.M., Nadler, R.B., Kozlowski, J.M., Perry, K.T., Kajdacsy-Balla, A., and Kittles, R. (2014). Vitamin D deficiency predicts prostate biopsy outcomes. Clin. Cancer Res. *20*, 2289–2299.

Murphy, A.B., Nyame, Y.A., Batai, K., Kalu, R., Khan, A., Gogana, P., Dixon, M., Macias, V., Kajdacsy-Balla, A., Hollowell, C.M., et al. (2017). Does prostate volume correlate with vitamin D deficiency among men undergoing prostate biopsy? Prostate Cancer Prostatic Dis. *20*, 55–60.

Nakamura, R.E.I., and Hackam, A.S. (2010). Analysis of Dickkopf3 interactions with Wnt signaling receptors. Growth Factors *28*, 232–242.

Nusse, R.A.L.X. (2020). Wnt target genes. https://web.stanford.edu/group/nusselab/cgi-bin/wnt/target_genes.

Peehl, D.M., Shinghal, R., Nonn, L., Seto, E., Krishnan, A.V., Brooks, J.D., and Feldman, D. (2004). Molecular activity of 1,25-dihydroxyvitamin D3 in primary cultures of human prostatic epithelial cells revealed by cDNA microarray analysis. J. Steroid Biochem. Mol. Biol. *92*, 131–141.

Peregrina, K., Houston, M., Daroqui, C., Dhima, E., Sellers, R.S., and Augenlicht, L.H. (2015). Vitamin D is a determinant of mouse intestinal Lgr5 stem cell functions. Carcinogenesis *36*, 25–31.

Pinho Christof Niehrs, S. (2007). Dkk3 is required for TGF-b signaling during Xenopus mesoderm induction. Differentiation *75*, 957–967.

Post, Y., Puschhof, J., Beumer, J., Kerkkamp, H.M., de Bakker, M.A.G., Slagboom, J., de Barbanson, B., Wevers, N.R., Spijkers, X.M., Olivier, T., et al. (2020). Snake Venom Gland Organoids. Cell *180*, 233–247 e221.

Prins, G.S., and Lindgren, M. (2015). Accessory sex glands in the male. In Knobil and Neill's Physiology of Reproduction, Fourth Edition, T.M. Plant and A.J. Zeleznik, eds. (Elsevier), pp. 773–797.

Prins, G.S., and Putz, O. (2008). Molecular signaling pathways that regulate prostate gland development. Differentiation *76*, 641–659.

Ramakrishnan, S., Steck, S.E., Arab, L., Zhang, H., Bensen, J.T., Fontham, E.T.H., Johnson, C.S., Mohler, J.L., Smith, G.J., Su, L.J., et al. (2019). Association among plasma 1,25(OH)2 D, ratio of 1,25(OH)2 D to 25(OH)D, and prostate cancer aggressiveness. Prostate *79*, 1117–1124.

Richards, Z., Batai, K., Farhat, R., Shah, E., Makowski, A., Gann, P.H., Kittles, R., and Nonn, L. (2017). Prostatic compensation of the vitamin D axis in African American men. JCI Insight *2*, e91054.

Richards, Z., McCray, T., Marsili, J., Zenner, M.L., Garcia, J., Manlucu, J.T., Voisine, C., Murphy, A.B., Prins, G.S., Murray, M., et al. (2019). Prostate stroma increases the viability and maintains the branching phenotype of human prostate organoids. iScience *12*, 304–317.

Robsahm, T.E., Tretli, S., Dahlback, A., and Moan, J. (2004). Vitamin D3 from sunlight may improve the prognosis of breast-, colon- and prostate cancer (Norway). Cancer Causes Control *15*, 149–158.

Romero, D., Kawano, Y., Bengoa, N., Walker, M.M., Maltry, N., Niehrs, C., Waxman, J., and Kypta, R. (2013). Downregulation of Dickkopf-3 disrupts prostate acinar morphogenesis through TGF-b/Smad signalling. J. Cell Sci. *126*, 1858–1867.

Ryan, S.D., Ferrier, A., and Kothary, R. (2012). A novel role for the cytoskeletal linker protein dystonin in the maintenance of microtubule stability and the regulation of ER-Golgi transport. Bioarchitecture *2*, 2–5.

Satija, R., Farrell, J.A., Gennert, D., Schier, A.F., and Regev, A. (2015). Spatial reconstruction of single-cell gene expression data. Nat. Biotechnol. *33*, 495–502.

Schmelz, M., Moll, R., Hesse, U., Prasad, A.R., Gandolfi, J.A., Hasan, S.R., Bartholdi, M., and Cress, A.E. (2005). Identification of a stem cell candidate in the normal human prostate gland. Eur. J. Cell Biol. *84*, 341–354.

Sharma Das, D., Wadhwa, N., Kunj, N., Sarda, K., Shankar Pradhan, B., and Majumdar, S.S. (2013). Dickkopf homolog 3 (DKK3) plays a crucial role upstream of WNT/b-CATENIN signaling for sertoli cell mediated regulation of spermatogenesis. PLoS One *8*, e63603.

Simons, B.W., Hurley, P.J., Huang, Z., Ross, A.E., Miller, R., Marchionni, L., Berman, D.M., and Schaeffer, E.M. (2012). Wnt signaling though beta-catenin is required for prostate lineage specification. Dev. Biol. *371*, 246–255.

Sneath, R.J., and Mangham, D.C. (1998). The normal structure and function of CD44 and its role in neoplasia. Mol. Pathol. *51*, 191–200.

Spielvogel, A.M., Farley, R.D., and Norman, A.W. (1972). Studies on the mechanism of action of calciferol. V. Turnover time of chick intestinal epithelial cells in relation to the intestinal action of vitamin D. Exp. Cell Res. *74*, 359–366.

Stahl, P.L., Salmen, F., Vickovic, S., Lundmark, A., Navarro, J.F., Magnusson, J., Giacomello, S., Asp, M., Westholm, J.O., Huss, M., et al. (2016). Visualization and analysis of gene expression in tissue sections by spatial transcriptomics. Science *353*, 78–82.

Studzinski, G.P., and Moore, D.C. (1995). Sunlight–can it prevent as well as cause cancer? Cancer Res. *55*, 4014–4022.

Takasato, M., Er, P.X., Chiu, H.S., and Little, M.H. (2016). Generation of kidney organoids from human pluripotent stem cells. Nat. Protoc. *11*, 1681–1692.

Tapia, C., Suares, A., De Genaro, P., and Gonzalez-Pardo, V. (2020). In vitro studies revealed a downregulation of Wnt/beta-catenin cascade by active vitamin D and TX 527 analog in a Kaposi's sarcoma cellular model. Toxicol. In Vitro *63*, 104748.

Tavera-Mendoza, L.E., Westerling, T., Libby, E., Marusyk, A., Cato, L., Cassani, R., Cameron, L.A., Ficarro, S.B., Marto, J.A., Klawitter, J., et al. (2017). Vitamin D receptor regulates autophagy in the normal mammary gland and in luminal breast cancer cells. Proc. Natl. Acad. Sci. U S A *114*, E2186–E2194.

Toivanen, R., and Shen, M.M. (2017). Prostate organogenesis: tissue induction, hormonal regulation and cell type specification. Development *144*, 1382–1398.

Untergasser, G., Koch, H.B., Menssen, A., and Hermeking, H. (2002). Characterization of epithelial senescence by serial analysis of gene expression: identification of genes potentially involved in prostate cancer. Cancer Res. *62*, 6255–6262.

Wagner, D., Trudel, D., Van der Kwast, T., Nonn, L., Giangreco, A.A., Li, D., Dias, A., Cardoza, M., Laszlo, S., Hersey, K., et al. (2013). Randomized clinical trial of vitamin D $_3$ doses on prostatic vitamin D metabolite levels and Ki67 labeling in prostate cancer patients. J. Clin. Endocrinol. Metab. *98*, 1498–1507.

Wang, H.H., Wang, L., Jerde, T.J., Chan, B.D., Savran, C.A., Burcham, G.N., Crist, S., and Ratliff, T.L. (2015a). Characterization of autoimmune inflammation induced prostate stem cell expansion. Prostate *75*, 1620–1631.

Wang, Y., Singhal, U., Qiao, Y., Kasputis, T., Chung, J.S., Zhao, H., Chammaa, F., Belardo, J.A., Roth, T.M., Zhang, H., et al. (2020). Wnt signaling drives prostate cancer bone metastatic tropism and invasion. Transl. Oncol. *13*, 100747.

Wang, Y., Hayward, S., Cao, M., Thayer, K., and Cunha, G. (2001). Cell differentiation lineage in

the prostate. Differentiation *68*, 270–279, https://doi.org/10.1046/j.1432-0436.2001.680414.x.

Wang, Z., Lin, L., Thomas, D.G., Nadal, E., Chang, A.C., Beer, D.G., and Lin, J. (2015b). The role of dickkopf-3 overexpression in esophageal adenocarcinoma. J. Thorac. Cardiovasc. Surg. *25*, 368–379.

Woo, T.C., Choo, R., Jamieson, M., Chander, S., and Vieth, R. (2005). Pilot study: potential role of vitamin D (Cholecalciferol) in patients with PSA relapse after definitive therapy. Nutr. Cancer *51*, 32–36.

Wright, A.S., Thomas, L.N., Douglas, R.C., Lazier, C.B., and Rittmaster, R.S. (1996). Relative potency of testosterone and dihydrotestosterone in preventing atrophy and apoptosis in the prostate of the castrated rat. J. Clin. Invest. *98*, 2558–2563.

Wu, X., Daniels, G., Shapiro, E., Xu, K., Huang, H., Li, Y., Logan, S., Greco, M.A., Peng, Y., Monaco, M.E., et al. (2011). LEF1 identifies androgen-independent epithelium in the developing prostate. Mol. Endocrinol. *25*, 1018–1026.

Xu, S., Zhang, Z.H., Fu, L., Song, J., Xie, D.D., Yu, D.X., Xu, D.X., and Sun, G.P. (2020). Calcitriol inhibits migration and invasion of renal cell carcinoma cells by suppressing Smad2/3-, STAT3- and beta-catenin-mediated epithelial-mesenchymal transition. Cancer Sci. *111*, 59–71.

Yamamoto, H., Masters, J.R., Dasgupta, P., Chandra, A., Popert, R., Freeman, A., and Ahmed, A. (2012). CD49f is an efficient marker of monolayer- and spheroid colony-forming cells of the benign and malignant human prostate. PLoS One *7*, 1–11.

Yang, J., Zhu, S., Lin, G., Song, C., and He, Z. (2017). Vitamin D enhances omega-3 polyunsaturated fatty acids-induced apoptosis in breast cancer cells. Cell Biol. Int. *41*, 890–897.

Yin, J., Yang, L., Xie, Y., Liu, Y., Li, S., Yang, W., Xu, B., Ji, H., Ding, L., Wang, K., et al. (2018). Dkk3 dependent transcriptional regulation controls age related skeletal muscle atrophy. Nat. Commun. *9*, 1752.

Yokoyama, N.N., Shao, S., Hoang, B.H., Mercola, D., and Zi, X. (2014). Wnt signaling in castration-resistant prostate cancer: implications for therapy. Am. J. Clin. Exp. Urol. *2*, 27–44.

Zenzmaier, C., Sampson, N., Plas, E., and Berger, P. (2013). Dickkopf-related protein 3 promotes pathogenic stromal remodeling in benign prostatic hyperplasia and prostate cancer. Prostate *73*, 1441–1452.

Zenzmaier, C., Untergasser, G., Hermann, M., Dirnhofer, S., Sampson, N., and Berger, P. (2008). Dysregulation of Dkk-3 expression in benign and malignant prostatic tissue. Prostate *68*, 540–547.

Zhang, K., Guo, Y., Wang, X., Zhao, H., Ji, Z., Cheng, C., Li, L., Fang, Y., Xu, D., Zhu, H.H., et al. (2017). WNT/beta-Catenin directs self-renewal symmetric cell division of hTERT(high) prostate cancer stem cells. Cancer Res. *77*, 2534–2547.

Zhang, K., Watanabe, M., Kashiwakura, Y., Li, S.A., Edamura, K., Huang, P., Yamaguchi, K., Nasu, Y., Kobayashi, Y., Sakaguchi, M., et al. (2010). Expression pattern of REIC/Dkk-3 in various cell types and the implications of the soluble form in prostatic acinar development. Int. J. Oncol. *151*, 414–420.

Zierold, C., Darwish, H.M., and DeLuca, H.F. (1995). Two vitamin D response elements function in the rat 1,25-dihydroxyvitamin D 24-hydroxylase promoter. J. Biol. Chem. *270*, 1675–1678.

iScience, Volume *24*

Supplemental Information

Vitamin D sufficiency enhances differentiation of patient-derived prostate epithelial organoids

Tara McCray, Julian V. Pacheco, Candice C. Loitz, Jason Garcia, Bethany Baumann, Michael J. Schlicht, Klara Valyi-Nagy, Michael R. Abern, and Larisa Nonn

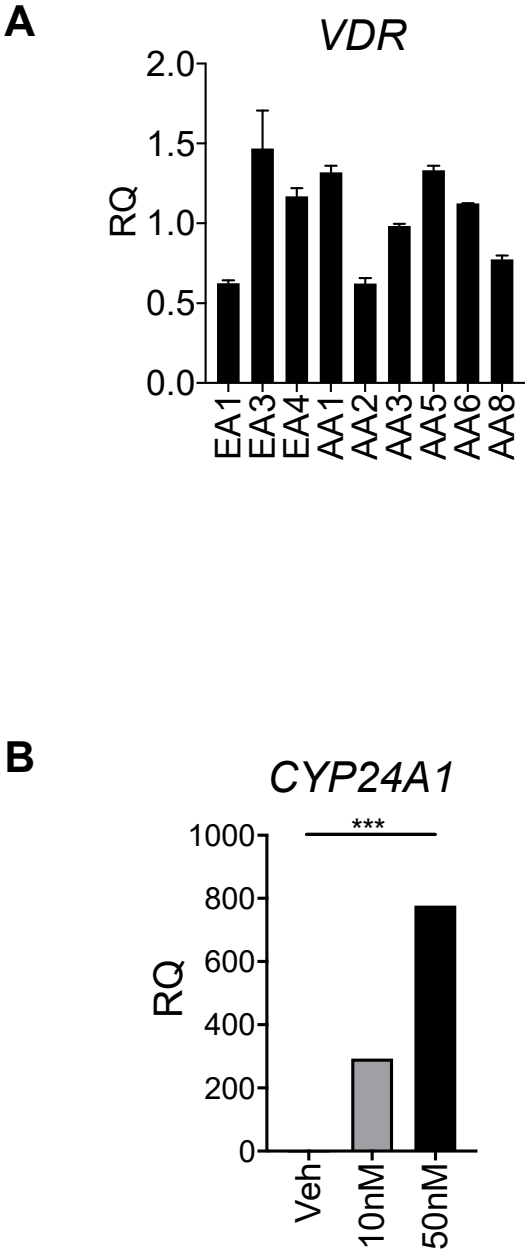

Supplemental Figure 1, related to Figure 1

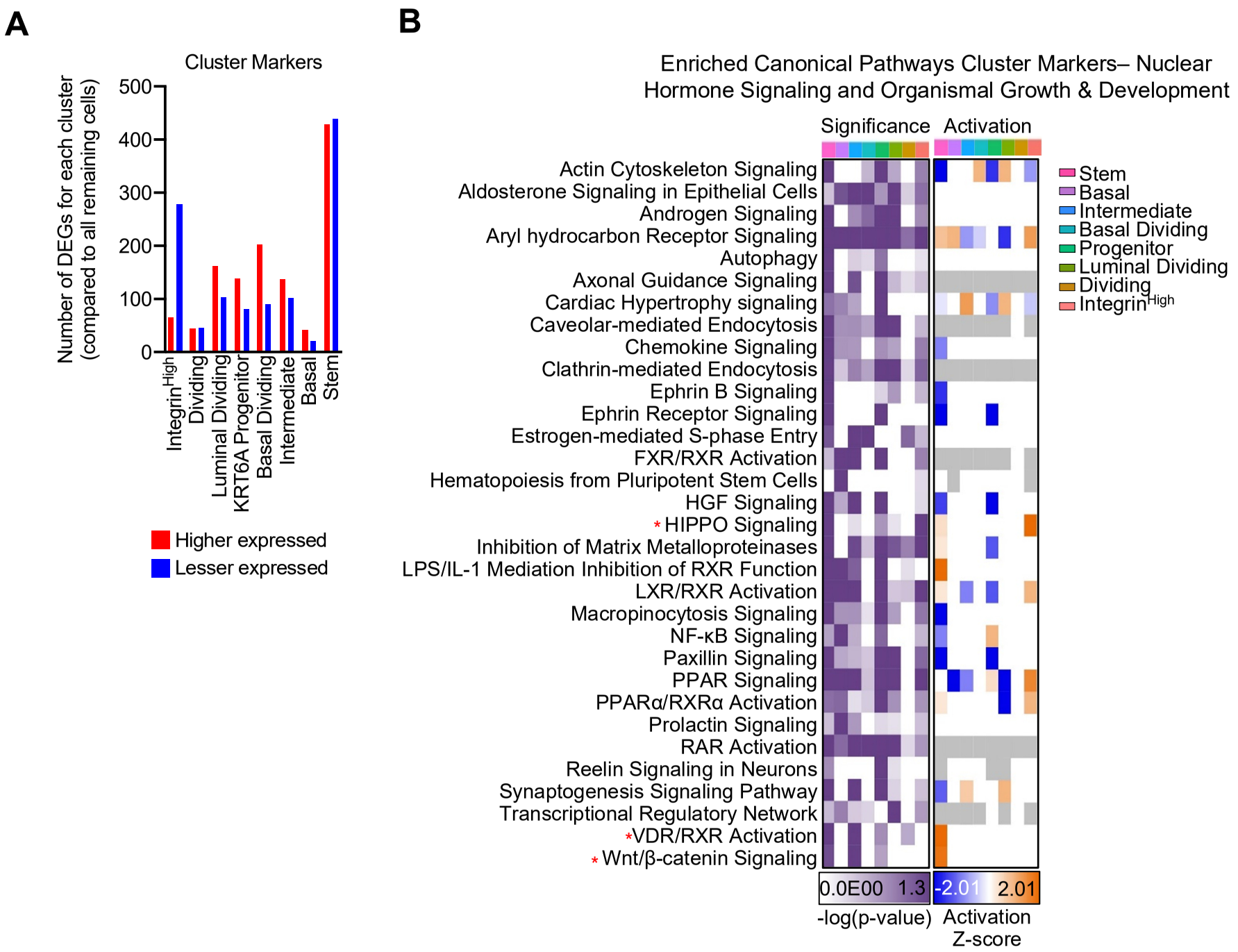

Supplemental Figure 2, related to Figure 2.

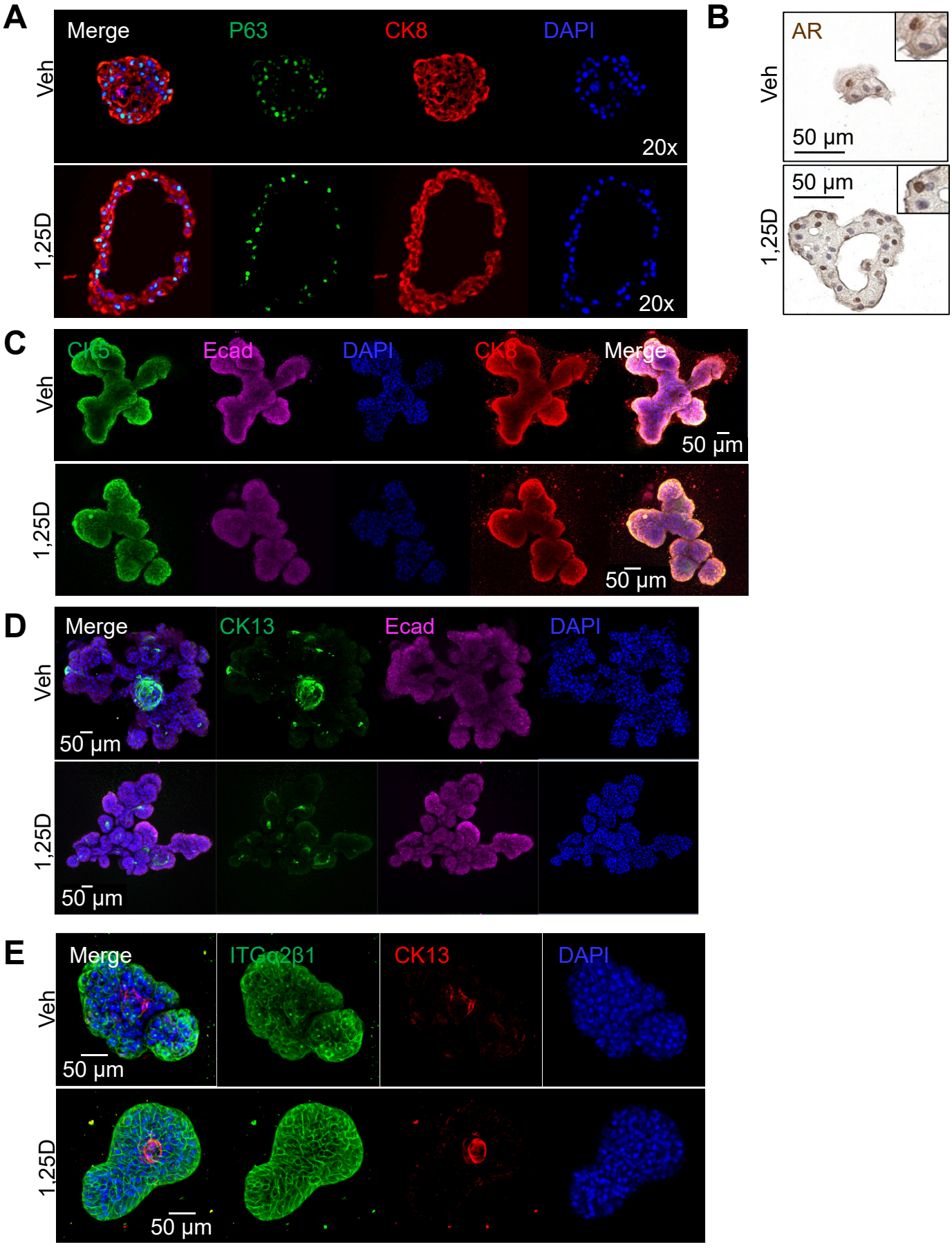

Supplemental Figure 3, related to Figure 2.

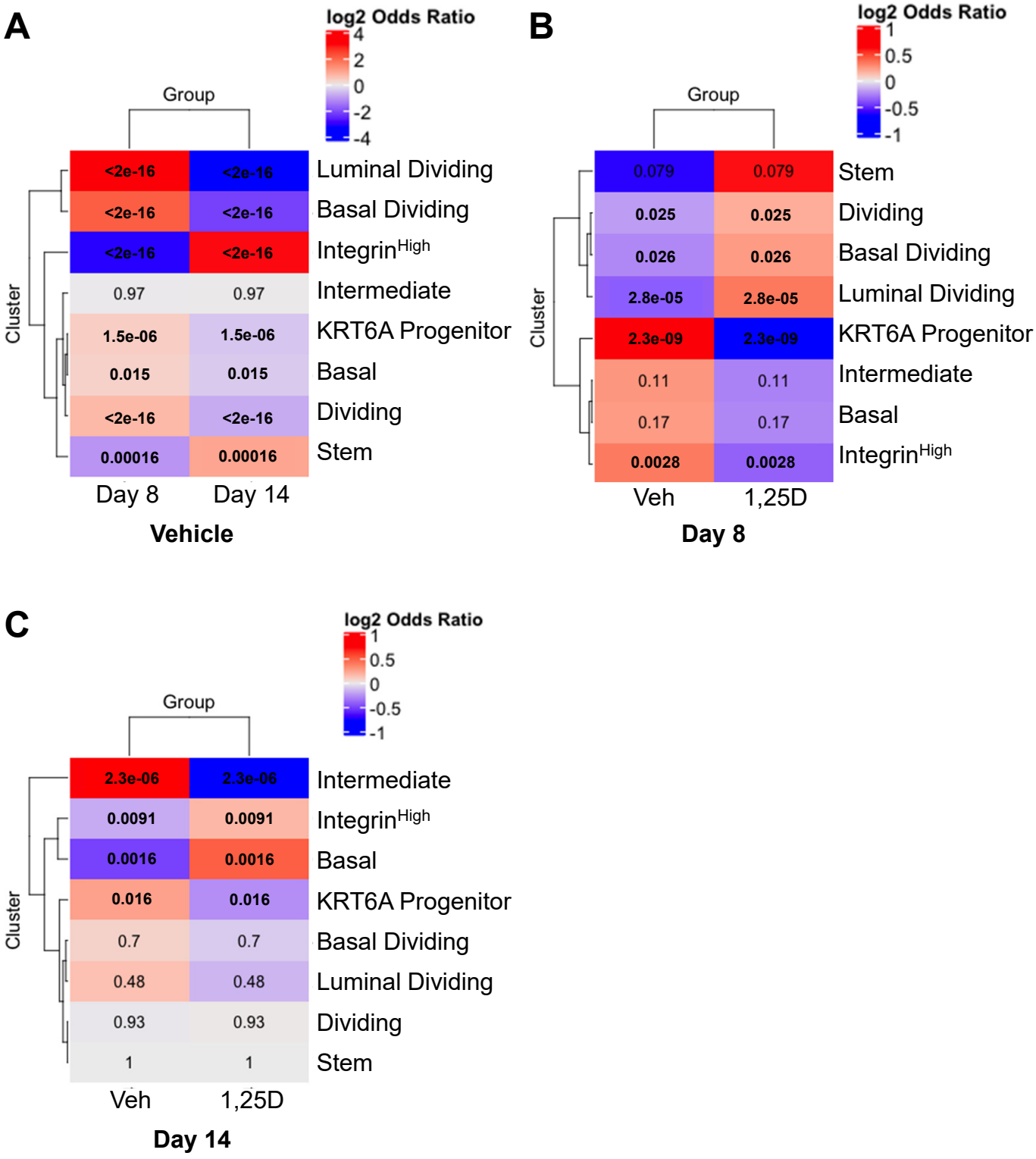

Supplemental Figure 4 (related to figure 2)

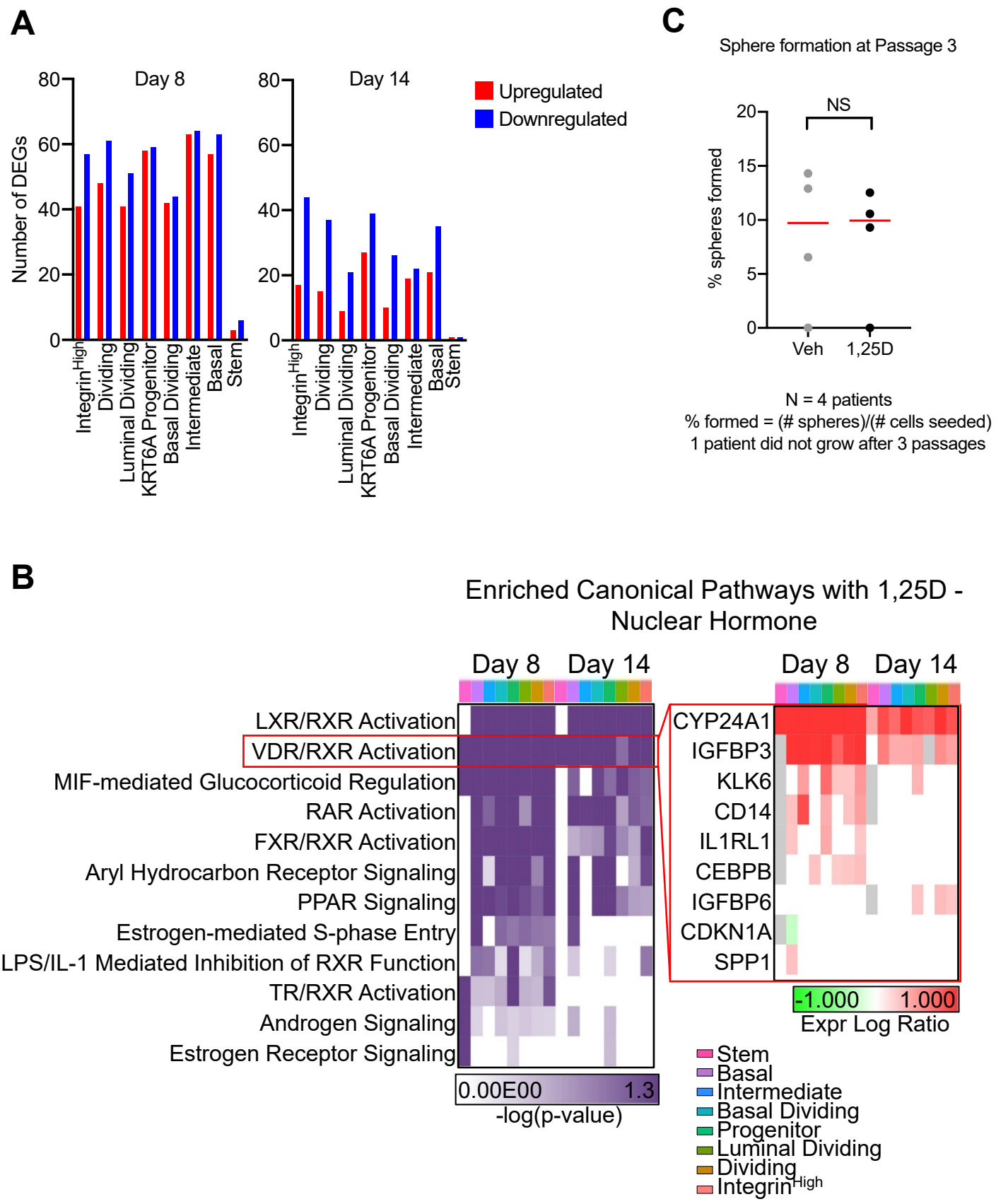

Supplemental Figure 5 (related to figure 3)

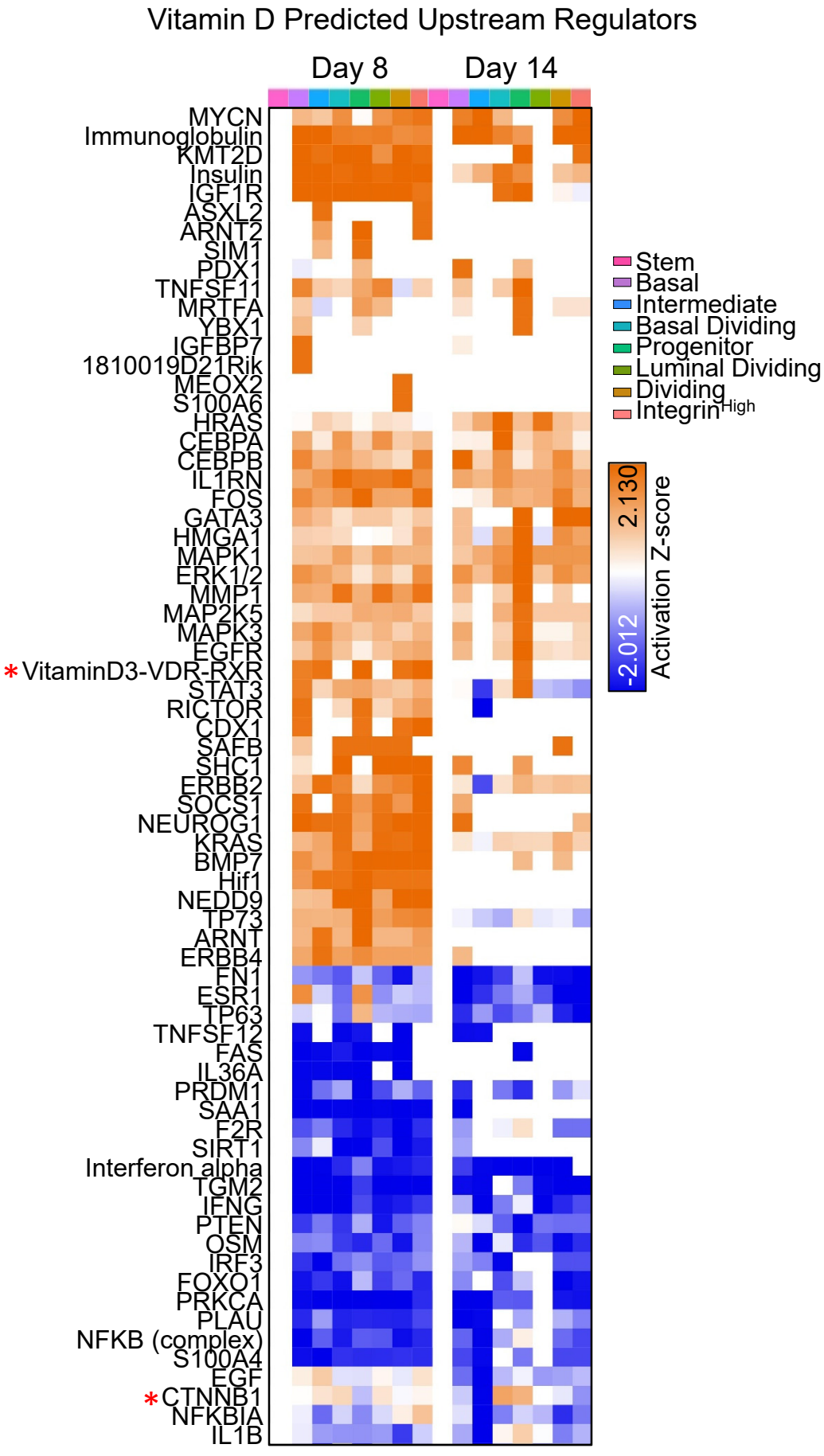

Supplemental Figure 6 (related to figure 3)

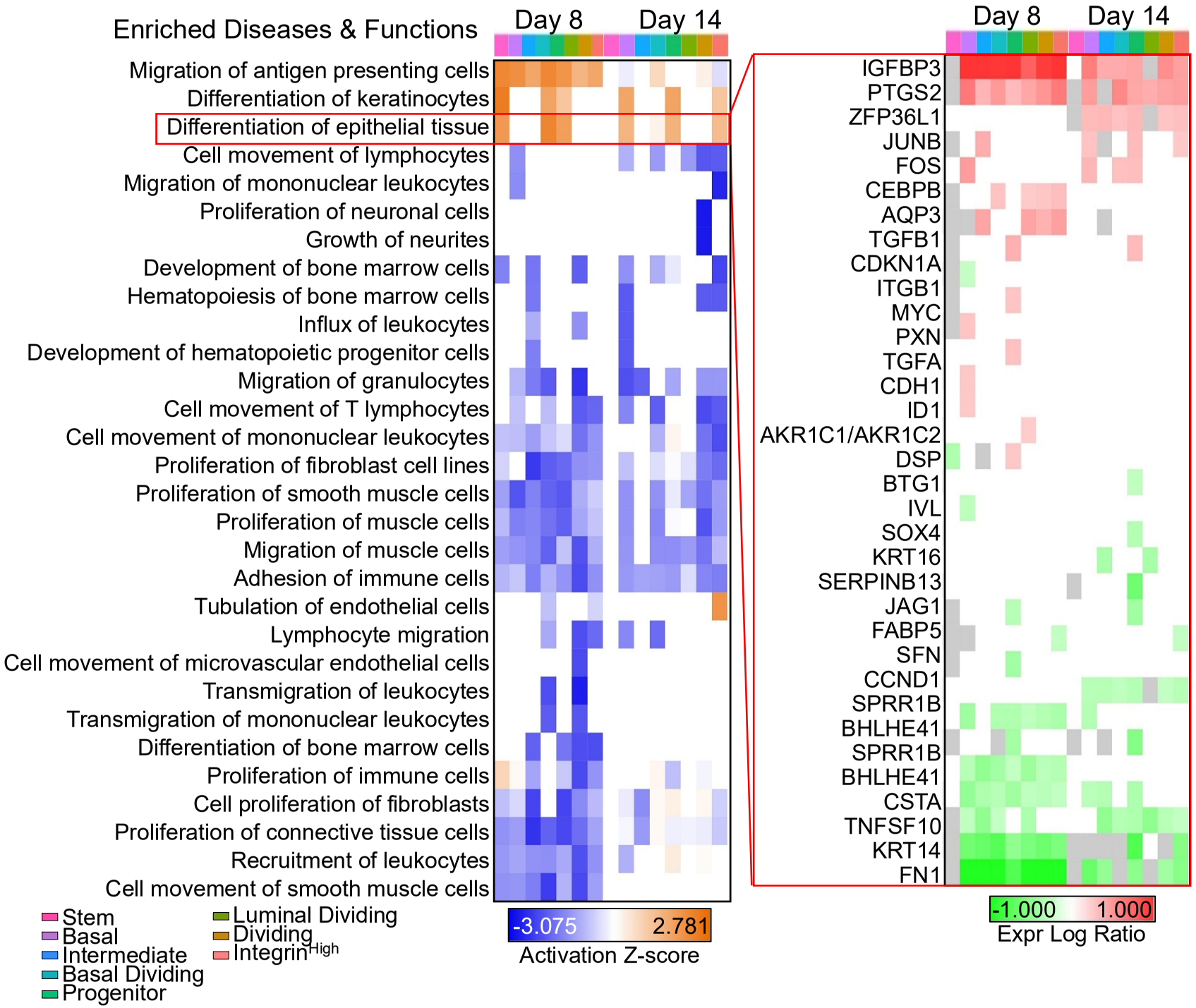

Supplemental Figure 7 (related to figure 3)

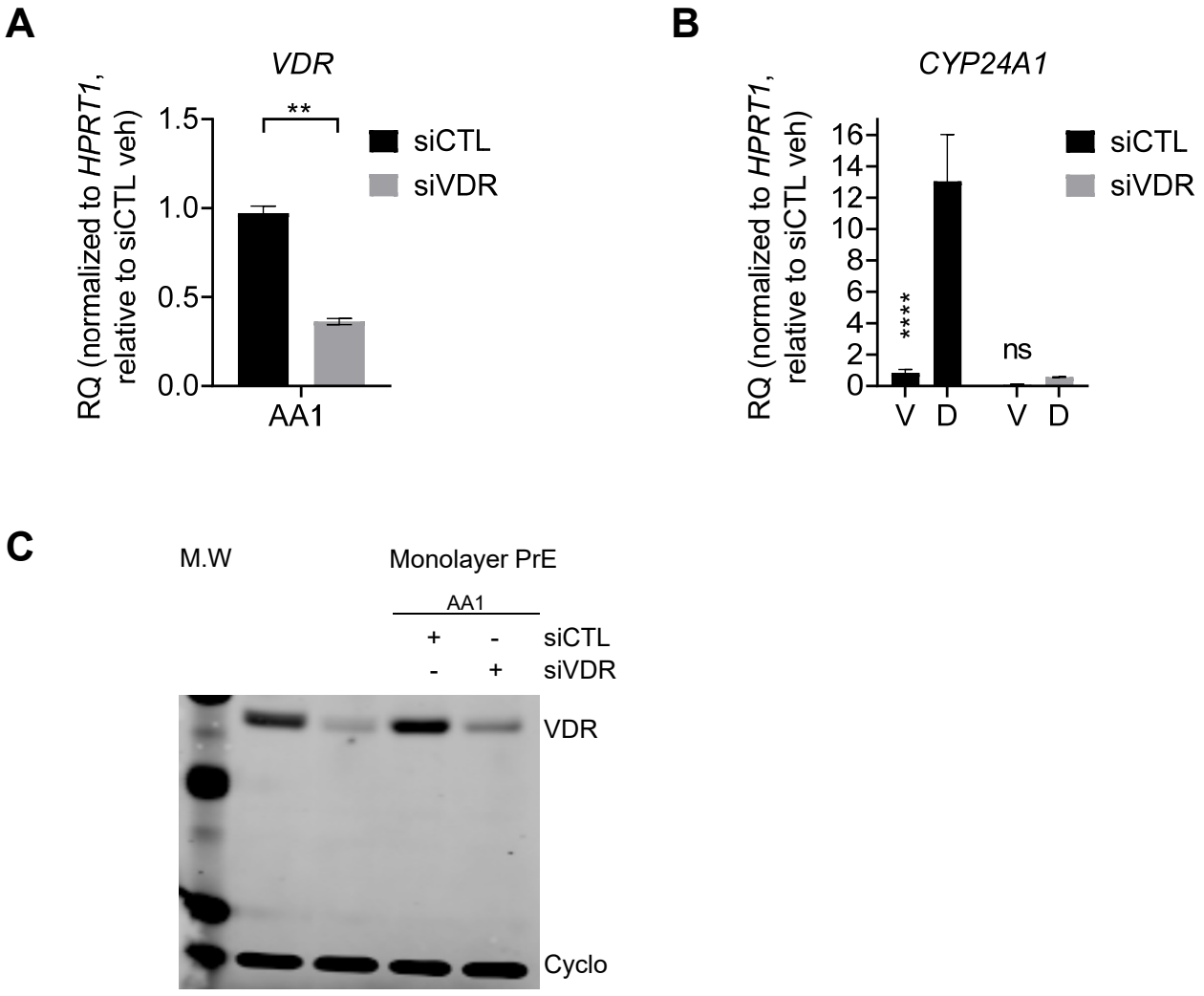

Supplemental Figure 8 (related to figure 3)

SUPPLEMENTAL INFORMATION TITLES AND LEGENDS

Supplemental Figure S1, related to Figure 1: PrE express VDR and organoids respond to 1,25D

(A) RT-qPCR of basal *VDR* expression in patient-derived prostate epithelial cells. Relative quantitation shown normalized to *HPRT1* (EA, European American; AA, African American; ancestries were patient self-declared). Error bars represent standard deviation of technical RT-qPCR pipetting replicates.

(B) RT-qPCR of *CYP24A1* expression in AA2 organoids cultured in vehicle, 10 nM or 50 nM 1,25D. Relative quantitation (RQ) shown normalized to *HPRT1.* Error bars represent standard deviation of RT-qPCR technical pipetting replicates, they are included but are small and difficult to visualize on scale of graph.

Supplemental Figure S2 (related to Figure 2): Pathway enrichment analysis for cluster markers.

(A) The number of markers per cluster. Cluster markers were identified by Seurat as genes having uniquely high or low expression in each cluster, compared to all other cells in the dataset. Markers that are highly expressed compared to all remaining cells are shown red, markers that are lesser expressed are blue.

(B) Cluster markers were input into IPA canonical pathway analysis. Significantly enriched pathways related to “Nuclear Hormone Signaling” and “Organismal Growth & Development” are shown. Dark purple is significant at $p<0.05$ for enrichment of each pathway (left) and activation z-score for each pathway (right).

Supplemental Figure 3 (related to figure 2): single channel IF images for FFPE (S3A, S3B) and whole-mounted (S3C-E) patient-matched organoids grown in vehicle (top) or 10nM 1,25D (bottom). Magnification and scale bars are shown on the images.

Supplemental Figure 4 (related to figure 2): Odds ratio (color) and corresponding p-value (number inset) comparing clusters between conditions. An odds ratio of 4 for Luminal Dividing cells (top right) means that there are ~4x more cells from the day 8 sample compared to day 14 than we would expect to see by chance.

(A) Comparison of day 8 and day 14 vehicle clusters.

(B) Comparison of vehicle and 1,25D clusters at day 8.

(C) Comparison of vehicle and 1,25D clusters at day 14.

Supplemental Figure S5 (related to Figure 3): Pathway enrichment analysis for Nuclear Hormone Signaling Pathways in differentially expressed genes with 1,25D treatment per cluster, per time point.

(A) The number upregulated (red) and downregulated (blue) differentially expressed genes (DEGs) with 1,25D compared to vehicle in each cluster at day 8 (left) and day 14 (right).

(B) For each cluster and time point, DEGs with 1,25D were input into IPA canonical pathway analysis. Enrichment for pathways related to “Nuclear Hormone Signaling” are shown. Scale represents –log(p-value) for enrichment of each pathway with 1,25D treatment (left) and expression log ratio with 1,25D treatment compared to vehicle (right). Red box shows differentially expressed genes related to VDR/RXR activation. Dark purple is significant at $p<0.05$.

(C) % of organoids formed at passage 3 from self-renewal assay for spheres grown in vehicle or 1,25D and split every 5-7 days. % of organoids formed was calculated by dividing the #

spheres at day 5 by the # cells at plating for passage 3. Each dot represents the outcome for a patient, 4 separate patients were tested. NS = not significant by Mann-Whitney t-Test for vehicle vs. 1,25D.

Supplemental Figure S6 (related to Figure 3): Upstream regulator analysis for differentially expressed genes with 1,25D treatment per cluster per time point. Top 70 significant regulators from IPA upstream regulator analysis of differentially expressed genes with 1,25D treatment per cluster. Scale represents predicated activation z-score.

Supplemental Figure S7 (related to Figure 3): Diseases & Functions Enrichment analysis for differentially expressed genes with 1,25D treatment per cluster per time point. Differentially expressed genes with 1,25D per cluster per time point were input into IPA Disease and Functions analysis. Significantly enriched Diseases & Functions related to “Molecular and Cellular Function, Physiological System Development and Function” are shown. Red box shows differentially expressed genes related to “Differentiation of Epithelial Tissue”. Scale represents activation z-score for enrichment (left) and expression log ratio with 1,25D compared to control (right).

Supplemental Figure S8 (related to Figure 3): siCTL and siVDR knockdown PrE cells

(A) RT-qPCR of *VDR* expression in AA1 monolayer PrE cells transduced with CTL or VDR siRNAs twice across 96 hours. Relative quantitation (RQ) shown normalized to *HPRT1* and scaled to siCTL veh sample per patient. Error bars represent standard deviation of RT-qPCR technical pipetting replicates. P value represents the outcome of a 2-way ANOVA for siCTL vs siVDR, **$p < 0.01$.

(B) RT-qPCR of *CYP24A1* expression in AA1 monolayer PrE cells transduced with CTL or VDR siRNAs twice across 96 hours. At 48 hours, cells were treated with vehicle or 10 nM 1,25D and cultured for 48 h prior to RNA collection. Relative quantitation (RQ) shown normalized to *HPRT1* and scaled to the vehicle sample of the siCTL virus. Error bars represent standard deviation of RT-qPCR technical pipetting replicates. P value represents the outcome of a 2-way ANOVA for vehicle vs. 1,25D, ****$p < 0.0001$.

(C) Full western blot for VDR and Cyclophilin-B (cyclo, housekeeper) in monolayer PrE cells that were transduced with CTL or VDR siRNAs as shown in Figure 3, molecular marker shown (M.W.)

TRANSPARENT METHODS

RESOURCE AVAILABILITY

Lead Contact

Further information and requests for resources and reagents should be directed to and will be fulfilled by the Lead Contact, Larisa Nonn (lnonn@uic.edu).

Material Availability

This study did not generate new unique reagents.

Data and Code Availability

ScRNAseq data has been submitted to NCBI Gene Expression Omnibus and can be found under accession number GSE142489. ChIP sequencing data can be found under accession number GSE124576. Spatial transcriptomics data can be found under accession number GSE159697.

EXPERIMENTAL MODEL AND SUBJECT DETAILS

Primary Cell Culture

Primary prostate cells were generated from fresh human male radical prostatectomy samples as previously described (Nonn, Peng et al. 2006, Giangreco and Nonn 2013). After obtaining informed consent from patients, tissue from benign regions of the peripheral zone were collected according to an IRB approved protocol of UIC Cancer Center Tissue Bank Core Facility (protocol # 2004-0679). A board-certified pathologist confirmed the tissue portion as benign from adjacent H&E section. Tissue was digested in collagenase/trypsin, and single cells were plated in Prostate Cell Growth Media (Lonza, Basel, Switzerland) to enrich for epithelial cells. At ~70% confluence, cells were frozen into multiple aliquots and cryopreserved for experiments. Epithelial purity was confirmed by RT-qPCR for expression of epithelial markers *KRT5*, *KRT8*, *KRT18,* and *TP63* (data not shown). Patient information is listed on **Table 1**. All cells were cultured at 37°C with 5% CO_2. Due to differences in patients' cells growth capacity and availability of cells, different patients were used for different endpoints.

Cell Lines

RWPE1 cells were purchased from ATCC in 2014, cryopreserved in low-passaged aliquots, re-authenticated in 2016, and used only at <20 passages. LAPC4 were generously donated from Dr. Charles Sawyers and grown in RPMI 1640 (Gibco, MD) with 10% fetal bovine serum on poly-lysine-coated flasks. 957E/hTERT cells were generously donated from Dr. Don Vander Griend. RWPE1 and 957E cells were grown in uncoated cell culture dishes in Keratinocyte Serum Free Media (Corning, NY). PC3 were purchased from ATCC, re-authenticated in 2013, and grown in RPMI 1640 (Gibco, MD) with 10% fetal bovine serum. All cells were cultured at 37°C with 5% CO_2.

Organoid Culture

Organoids were grown as previously described by our group (McCray, Richards et al. 2019, Richards, McCray et al. 2019). Briefly, primary prostate epithelial cells were established and cryopreserved from benign regions of the peripheral zone of radical prostatectomy patients (men aged 50-75), according to an IRB approved protocol of UIC Cancer Center Tissue Bank Core Facility (Protocol # 2004-0679)(Peehl 2003). Cells were thawed and grown to passage 2 on collagen-coated dishes to ~70% confluency. Epithelial cells were plated singly and sparsely (100–1,000 cells per well, depending on patient-specific growth ability) in 100 µL of 10%–50% growth factor-reduced Matrigel (Corning, NY). To prevent cells from adhering to the bottom and growing as a monolayer, cells were plated over a 50% Matrigel base layer in a 96-well plate or low-attachment 96-well plate without a base layer. Matrigel was diluted with organoid growth media containing Keratinocyte Serum Free Media (Gibco, MD), bovine pituitary extract, and epidermal growth factor, supplemented with 5% charcoal-stripped fetal bovine serum and 10 nM dihydrotestosterone (DHT). After Matrigel solidified, 100 µL of organoid growth media was added to each well and was refreshed every 1–3 days. Media was supplemented with vehicle or 1,25D, and cells as indicated in figure legends. Given the patient heterogeneity in growth capacity, cells were collected at subtly different time points.

Prostate tissue slice explant cultures

Fresh tissue from benign regions of the peripheral zone of radical prostatectomy patients (men aged 50-75) was collected according to an IRB approved protocol of UIC Cancer Center Tissue Bank Core Facility (Protocol # 2004-0679) using a 5mm dermatology round punch. A board-certified pathologist confirmed the tissue portion as benign from adjacent H&E section. Tissue slice explant method was adapted from Maund et al (Maund, Nolley et al. 2014). Tissue was precision sliced into 300-micron sections using an Alabama Tissue Slicer (Alabama Research and Development) and placed on titanium inserts within a 6-well plate and maintained in 2.5mL KSFM supplemented with with 5% v/v charcoal stripped FBS. For deficient vitamin D a vehicle control (<0.01% EtOH) was added to media, for sufficient vitamin D the circulating form of the hormone (25D) was used to mimic tissue- and organ-level conditions. Plate is attached to a fixed angle rotor to gently rotate the tissues in an out of media during culture.

METHOD DETAILS

Cell Treatments

Monolayer and organoid primary cells and monolayer cell lines were maintained in media as described above. Cells were treated with vehicle or 10 nM or 50 nM 1,25D (active hormone) over the course of culture, as indicated in figure legends. For Wnt induction, cells were treated with vehicle or 9 μM Chiron for 5 h before collection. For rDKK3 (1118-DK-050, R & D Systems, MN), cells were exposed to 50 ng/mL over the course of culture, as indicated in figure legends.

Brightfield Image Acquisition, Processing, and Analysis

Images of organoid cultures were acquired and analyzed as previously described by our group (McCray, Richards et al. 2019, Richards, McCray et al. 2019). Briefly, images were captured at 4x magnification using the Evos FL Auto 2 Imaging System (Thermo Fisher Scientific, MA), and up to 50 z-planes were captured per quadrant of a 96-well plate. Images of each quadrant were stitched together at each z-position, and z-stacks were compressed to an enhanced depth-of-field

image using Celleste Image Analysis software to visualize each organoid in the well within a single image (Thermo Fisher Scientific, MA). Images were also collected at 10x and 20x of individual organoids for better resolution for figures.

Organoid morphology: Solid, translucent and acinar organoids were counted per well for n ≥ 3 wells of each condition for 10 patients, and the percentage of each morphology was calculated. Percentage average and standard error of the mean was determined for the 7 patients that were capable of forming all three types of morphologies.

Organoid number and area: Organoid count and area metrics were generated by manual identification of each organoid using Celleste Image Analysis software. At least three wells per patient were analyzed for technical replicates, each patient had 1-4 biological replicates performed by thawing vials for repeat experiments from each patient, and each patient serves as a biological replicate for the phenotype. Area was measured at roughly day 14, +/- 4 days. Area was normalized to vehicle control, and a non-parametric, one-sided unpaired, Mann Whitney t-test was used to compare between treatments, $p<0.1$ was considered significant.

Self-renewal assay

Replating self-renewal assay was performed to assess stem cell sphere formation ability. Epithelial cells were plated singly and sparsely (100–1,000 cells per well, depending on patient-specific growth ability) in 100 µL per well of 10% growth factor-reduced Matrigel (Corning, NY) on a low-attachment 96-well plate without a base layer. Matrigel was diluted with organoid growth media containing Keratinocyte Serum Free Media (Gibco, MD), bovine pituitary extract, and epidermal growth factor, supplemented with 5% charcoal-stripped fetal bovine serum and 10 nM dihydrotestosterone (DHT). After Matrigel solidified, 100 µL of organoid growth media was added to each well and was refreshed every 1–3 days. Media was supplemented with vehicle or 1,25D, and cells were grown for 5-7 days in culture. After spheres formed, they were dissociated into single cells using TryPLE and replated in the same conditions for another passage, up to passage 3. Cells were imaged at the day of plating to determine the number of cells seeded and imaged

at day 5-7 to determine the number of spheres formed. The % of spheres formed was determined by dividing the number of spheres by the number of cells seeded.

Immunostaining

Immunostaining was performed as previously described by our group (McCray, Richards et al. 2019). Organoids were collected from Matrigel by Dispase (Stemcell Technologies, MA), resuspended in HistoGel (Thermo Fisher Scientific, MA), fixed in 4% paraformaldehyde, and paraffin-embedded. Whole-mounted organoids were transferred by pipette to a chamber slide, fixed in 4% paraformaldehyde, and permeabilized. GFP signal in transduced cells was quenched with 50 mM NH_4Cl if 488-channel was used for immunostaining. Sections (5 μm) of embedded organoids or whole-mounted organoids were incubated overnight at 4°C with rabbit monoclonal anti-p63a antibody (D2K8X, Cell Signaling Technology, MA), polyclonal guinea pig anti-cytokeratin 8/18 (03-GP11, American Research Products Inc, MA), monoclonal rabbit anti-cytokeratin 13 (ab92551, Abcam, UK), monoclonal rabbit anti-androgen receptor (D6F11, Cell Signaling Technology, MA), monoclonal rabbit anti-β-catenin (8480, Cell Signaling Technology, MA), monoclonal mouse anti-integrin α2/β1 (ab20483, Abcam, UK), polyclonal rabbit anti-keratin 5 (905501, BioLegend, CA), or monoclonal rabbit anti-DKK3 (ab186409, Abcam, UK). Samples were incubated with Alexa Fluor conjugated secondaries for 1 h at room temp or overnight at 4°C. Samples were counterstained with Alexa Fluor 647-phalloidin and DAPI, when appropriate. For whole-mount staining of cytokeratin 13 and DKK3, incubation with unconjugated monoclonal rabbit anti-DKK3 (ab186409, Abcam, UK) and secondary antibody was performed, followed by incubation with conjugated monoclonal rabbit anti-cytokeratin 13 (EPR3671 conjugated to Alexa Fluor 647, ab198585, Abcam, UK) and counterstaining. Edu staining was performed as previously described (McCray, Moline et al. 2019).

Immunostaining Quantification

Positive and negative nuclei for β-catenin staining were manually identified from two fields of view images for each condition. Number of nuclei was identified from DAPI and positive nuclei were identified by localization of red β-catenin for each cell in the field of view.

Lentivirus Transduction

Cells were transduced by centrifugation (Xin, Ide et al. 2003) with DKK3 siRNA/shRNAi Lentivirus (iV006166) or scrambled siRNA GFP Lentivirus (LVP015-G) (Applied Biological Materials Inc., CA) and selected by passaging at least once into media containing 1–3 μg/mL puromycin until all cells were GFP+ before plating into Matrigel.

SiRNA Transfection

PrE AA1 cells were transiently transfected as previously described (Blajszczak and Nonn 2019). Briefly, cells were plated on a 60 mm dish and transfected with a pool of three 19-25 siRNA sequences against VDR (sc-106692) or control siRNAs (sc-37007) (Santa Cruz Biotech, TX) using DharmaFECT Duo Transfection Reagent (T-2005-01) (Horizon Discovery, UK). Cells were plated and given 24 hours to attach and divide. At 24 h, siRNAs were added and incubated for 48 h to allow siRNA incorporation and inhibition of VDR translation. After 48 h, a second siRNA delivery was performed along with 1,25D treatments. Cells were collected after 48 h with 1,25D, and 96 h with siRNAs. Prior to RNA collection, Chiron was added for 5 h for the *AXIN2* assay, as described in the cell treatments section. Protein was also collected to validate knockdown.

Cell Sorting

Day-14 organoids from AA1 were dissociated with Dispase and TrypLE Express Enzyme (Gibco, MA) to generate single-cell suspensions and were fixed with ethanol. Cells were incubated with Alex Fluor 647-conjugated monoclonal rat anti-CD49f (BioLegend, CA), PE-conjugated monoclonal mouse anti-CD26 (BioLegend, CA), and PacificBlue-conjugated monoclonal mouse anti-Ki67 (BioLegend, CA) antibodies and were sorted with LSR Fortessa (BD Biosciences, CA). FlowJo software (FlowJo LLC, OR) was used to create scatterplot overlays of samples at each time point.

For live cell sorting for RT-qPCR array, day-17 organoids were dissociated as described above and incubated with Alex Fluor 647-conjugated monoclonal rat anti-CD49f (BioLegend, CA) and FITC-conjugated monoclonal mouse anti-CD26 (BioLegend, CA) antibodies. Cells were live-sorted with the MoFlo sorter (Beckman-Coulter, CA) directly into TRIzol (Thermo Fisher Scientific, MA) for RNA isolation.

PCR Profiling Arrays and RT-qPCR gene expression

For PCR profiling array, organoid RNA was isolated using TRIzol extraction. RNA quantity and quality were determined by NanoDrop Spectrophotometer (Thermo Fisher Scientific, MA). cDNA was generated with Qiagen RT^2 First Strand Kit (Qiagen, Germany), and gene expression was assessed using RT^2 Profiler PCR Array Human WNT Signaling Pathway Plus (PAHS-043YC-2, Qiagen Germany). Arrays were run on QuantStudio6 (Thermo Fisher Scientific, MA) and normalized independently using five reference genes according to the manufacturer's protocol. The $\Delta\Delta$CT method was used for comparative analysis (Livak and Schmittgen 2001).

For individual RT-qPCR, RNA was isolated with TRIzol and reverse-transcribed using a High Capacity cDNA Reverse Transcription Kit (Thermo Fisher Scientific, MA), qPCR was performed on the QuantStudio6 machine with SYBR green. Expression of *VDR* was quantified using forward primer 5'- GACCTGTGGCAACCAAGACT-3' and reverse primer 5'-GAACTTGATGAGGGGCTCAA-3'. Expression of *CYP24A1* was quantified using forward primer 5'- CATTTTAGCAGTCAGCTCCCG-3' and reverse primer 5'-GGCAACAGTTCTGGGTGAAT-3'. Expression of *AXIN2* was quantified using forward primer 5'-AGTGTGAGGTCCACGGAAAC-3' and reverse primer 5'-ACAGGATCGCTCCTCTTGAA-3'. Expression of *DKK3* was quantified using forward primer 5'-TCACATCTGTGGGAGACGAA-3' and reverse primer 5'-CTGGCAGGTGTACTGGAAGC-3'. Gene expression was normalized to the reference gene *HPRT1* with forward primer 5'-TGCTGACCTGCTGGATTACA-3' and reverse primer 5'-CTGCATTGTTTTGCCAGTGT-3'.

Western Blot

Organoids were collected from Matrigel, lysed in cell lysis buffer (9803, Cell Signaling, MA) with protease/phosphatase inhibitor (5872, Cell Signaling, MA), and sonicated. Bradford assay was used to detect protein concentration. Protein was denatured before separation on 1.5 mm 4%–12% NuPAGE Bis-Acrylamide gels with NuPAGE MOPS SDS running buffer and NuPage antioxidant (Thermo Fisher Scientific, MA). Gels were primed for 10 min at 100 V and run for 1 h at 125 V. Proteins were transferred from gels to 42-µm-pore Millipore PVDF membranes (Sigma-Aldrich, MO) for 1 h at 30 V. Protein membranes were blocked using Odyssey Blocking Buffer (LI-COR Biosciences, NE). Primary antibodies were diluted in Odyssey Blocking Buffer and incubated with blots overnight at 4ºC. Primary antibodies used include monoclonal mouse anti-cyclophilin-B (CL3901, Abcam, UK), monoclonal rabbit anti-VDR (D2K6W, Cell Signaling, MA), monoclonal rabbit anti-DKK3 (ab186409, Abcam, UK), and monoclonal mouse anti-GAPDH (MAB374, Millipore Sigma, MA). Secondary antibodies IRDye 800CW anti-mouse IgG (926-32210, LI-COR Biosciences, NE) and IRDye 680RD anti-rabbit IgG (926-68071, LI-COR Biosciences, NE) were diluted in Odyssey Blocking Buffer and incubated with blots for 1 h at room temperature. Blots were imaged using the LI-COR Odyssey Imaging system.

DKK3 ELISA

Primary epithelial cells were grown as monolayers and treated with vehicle or 10 nM 1,25D for 72 h, with treatments refreshed every 24 h. At 48 h, cells were washed, and media depleted in bovine pituitary extract was added to prevent detecting exogenous bovine DKK3. Media was collected at 72 h, and cells were counted with a Cellometer Automated Cell Counter (Nexcelom, MA) for normalization. Protein was quantified using Human Dkk-3 DuoSet Solid Phase Sandwich ELISA (DY1118, R&D Systems, MN), per manufacturer's instructions. Plates were read using Synergy HTX Multi-mode Read (BioTek, VT).

scRNAseq

Organoids were collected by Dispase and TrypLE as described above, and scRNAseq was performed as previously described (McCray, Moline et al. 2019). Briefly, cell number and viability

were determined using the Cellometer Automated Cell Counter (Nexcelom, MA) by Trypan Blue exclusion. Samples were >85% viable cells, and ~5,000 cells per sample were captured with the 10x Chromium chip (10x Genomics, CA). Libraries were prepared per manufacturer's instructions using the 3' Transcript Capture and Single Cell Library Prep v3 chemistry (10x Genomics, CA). Libraries were quantified and titrated by MiSeq (Illumina, CA) into an even pool and sequenced across one 2x150nt lane of the NovaSeq 6000 (Illumina, CA) at a depth of ~50,000 reads per cell. Library titration and sequencing was performed by University of Illinois at Urbana-Champaign (UIUC) DNA services. scRNAseq samples were processed and aligned to Ensembl genome GRCh38 using the Cell Ranger 3.2.1 pipeline (10x Genomics, CA) by UIUC DNA Services.

Seurat Integration and Clustering Analysis

The CellRanger output was loaded into Seurat 3.1.0 for clustering, following integration and differential gene expression workflows (Satija, Farrell et al. 2015, Butler, Hoffman et al. 2018). Poor-quality cells with high mitochondrial gene expression and unusually high or low reads were subset out of the dataset to remove dying cells and doublets. Individual samples were normalized, cell cycle and mitochondrial features were scored, and data was scaled. Next, samples were integrated to find similar cells across samples, and cell cycle and mitochondrial features were regressed. Highly variable features were used for principal component analysis and reduction for UMAP clustering. We reduced 30 principal components at a resolution of 0.4 to obtain a UMAP plot with a modularity of 0.8249. Clusters were assigned epithelial identities based on expression of known epithelial markers, as previously described (McCray, Moline et al. 2019). Cluster markers were determined by DEGs in each cluster compared to all remaining cells, determined by Seurat default non-parametric Wilcoxon rank sum test (Butler, Hoffman et al. 2018). Similarly, DEGs with 1,25D treatment compared to vehicle controls were determined for each cluster at both time points in the same fashion. Genes with adjusted $p < 0.05$ after Bonferroni correction were considered significant. Log2 odds ratio (color) and corresponding p-value (number inset)

were determined from Fisher's exact test comparing each cluster to all other clusters between conditions.

Monocle Pseudotime Analysis

CellRanger outputs for day-8 and day-14 vehicle data were loaded into Monocle 3 and combined, and pseudotime trajectories were constructed following the Trapnell lab's workflow (Trapnell, Cacchiarelli et al. 2014, Qiu, Mao et al. 2017, Cao, Spielmann et al. 2019). Briefly, data were loaded and normalized, samples were combined, batch effects were removed, cells with high mitochondrial gene expression were removed, and trajectories were constructed. The beginning node was selected based off of *KRT13* expression.

Ingenuity Pathway Analysis (IPA)

Lists of cluster markers and DEGs with 1,25D treatment that were generated in Seurat were analyzed with IPA (Qiagen, https://www.qiagenbioinformatics.com/products/ingenuitypathway-analysis). Gene lists were input into the core analysis function to determine canonical pathways, Diseases & Functions, and Upstream Regulators. Only cluster markers and DEG genes with adjusted $p < 0.05$ from Seurat's default non-parametric Wilcoxon rank sum test were used. Once each core analysis was finished, a comparative analysis was performed for each pathway, function or Upstream Regulator across each cluster at each time point.

VDR ChIP Sequencing

ChIP sequencing for VDR-bound DNA near the *DKK3* promoter was observed in a previously published dataset of 1,25D-treated PrE cells from our lab (Baumann, Lugli et al. 2019), deposited at NCBI GEO accession number GSE124576.

Spatial gene expression profiling of tissue slices

Tissue slices were cultured in this medium with the addition of 0.01% EtOH (vehicle control) or 50nM 25D for 8 hours. Tissue slices were embedded in OCT and flash-frozen in an isobutane bath surrounded in liquid nitrogen. Frozen sections (10 μm) were placed onto a 10X Genomics Visium experimental slide and processed per manufacturer's instructions. Briefly, the tissue is

was fixed with methanol, stained with Hematoxylin and Eosin, and imaged with Brightfield imaging prior to tissue permeabilization for 30 min. Reverse transcription reagents were added to initiate first strand cDNA that occurred on the slide. cDNA was transferred to a tube and quantified and used for library workflow. Following second strand synthesis double-stranded cDNA was quantified by qPCR. Peak RFU value at 25% required 19 amplification cycles. For library construction, fragmentation of the cDNA followed by a double-sided SPRI cleanup, selected for optimally sized cDNA amplicons. End repair and A-tailing prepped the 3' end of the cNDA adaptors in order to add adaptors for the partial 2 read sequence. cDNA fragments were amplified in a bulk sample index PCR reaction. The total number of sample index number PCR cycles were selected based on carried forward 25% of total cDNA mass into the fragmentation reaction. Enzymatic fragmentation and double sides SPRI selection were performed to optimize cDNA amplicon size using an Agilent TapeStation analysis. Sequencing was performed at UIUC using the NovaSeq, SP, Paired-reads, 2X150bp. Recommended sequencing parameters were performed according to the manufacturer's suggestions. Libraries were quantified and titrated by MiSeq (Illumina, CA) into an even pool and sequenced across one 2x15bp lane of the NovaSeq 6000 (Illumina, CA) at a depth of ~50Urbana-Champaign (UIUC) DNA services.

Spatial gene expression analysis

Spatial .json maps were created manually in Loupe (10x Genomics) to exclude areas of folded tissue. Spatial .json and sequence files were processed and aligned to Ensembl genome GRCh38 using the SpaceRanger pipeline (10x Genomics, CA) by UIUC DNA Services. Normalized aggregated files were analyzed in Loupe (10X Genomics). Areas of epithelium were selected and a gene lists were compared between samples by log2 expression with locally distinguishing significant feature comparison. Loupe generated heatmaps with statistics and violin plots. P-values are adjusted using Benjamin-Hoschberg correction for multiple tests.

QUANTIFICATION AND STATISTICAL ANALYSIS

Statistical analyses were performed with GraphPad Prism version 8 (GraphPad Software Inc., CA), Microsoft Excel (Microsoft Windows, WA), Seurat R Package (Butler, Hoffman et al. 2018), and IPA software (Qiagen Bioinformatics, DK); details can be found in figure legends. A non-parametric, one-sided unpaired, Mann Whitney U-test was used to compare organoid area. For RT-qPCR and ELISA analyses a 2-way ANOVA was used to compare conditions, standard deviation of replicates or standard error of mean is depicted by error bars as noted in the figure legends. Differential expression analysis was performed with Seurat, using a non-parametric Wilcoxon rank sum test, and adjusted Bonferroni corrected $p < 0.05$ was considered significant. $P < 0.05$ was used as a significant for IPA enriched pathway analysis.

KEY RESOURCES TABLE

REAGENT or RESOURCE	SOURCE	IDENTIFIER
Antibodies		
rabbit monoclonal anti-p63a antibody	Cell Signaling	Cat #: 56687, RRID#: AB_2799516
polyclonal guinea pig anti-cytokeratin 8/18	American Research Products Inc	Cat #: 03-GP11, RRID#: AB_1541064
monoclonal rabbit anti-cytokeratin 13	Abcam	Cat #: ab92551 RRID#: AB_2134681
monoclonal rabbit anti-androgen receptor	Cell Signaling	Cat #: 5153 RRID#: AB_10691711
monoclonal mouse anti-integrin α2/β1	Abcam	Cat #: ab30483 RRID#: AB_775705
monoclonal rabbit anti-β-catenin	Cell Signaling	Cat #: 8480 RRID#: AB_11127855
monoclonal rabbit anti-DKK3	Abcam	Cat #: ab186409
Alexa Fluor 647 conjugated monoclonal rabbit anti-cytokeratin 13	Abcam	Cat #: ab198585
monoclonal mouse anti-cyclophilin-B	Abcam	Cat #: CL3901 RRID:AB_2787028
monoclonal rabbit anti-VDR	Cell Signaling	Cat #: D2K6W RRID:AB_2637002
monoclonal anti-GAPDH antibody clone 6C5	Millipore Sigma	Cat #: MAB374 RRID#: AB_2107445
Alex Fluor 647-conjugated monoclonal rat anti-CD49f	BioLegend	Cat #: 313609 RRID#: AB_493636
FITC-conjugated monoclonal mouse anti-CD26	BioLegend	Cat #: 302704 RRID#: AB_314288
PE-conjugated monoclonal mouse anti-CD26	BioLegend	Cat #: 302705 RRID#:AB_314289
PacificBlue-conjugated monoclonal mouse anti-Ki67	BioLegend	Cat #: 652421 RRID#: AB_2564489
Bacterial and Virus Strains		
DKK3 siRNA/shRNAi Lentivirus	Applied Biological Materials Inc.	Cat #: iV006166
scrambled siRNA GFP Lentivirus	Applied Biological Materials Inc.	Cat #: LVP015-G
Biological Samples		
N/A	N/A	N/A
Chemicals, Peptides, and Recombinant Proteins		
1α,25-Dihydroxyvitamin D3 (vitamin D)	Enzo Life Sciences	Cat #: BML-DM200-0050 RRID#:
Recombinant DKK3	R&D Systems	Cat #: 1118-DK-050 RRID#:
Chir99021 (Chiron)	STEMCELL Technologies	Cat #: 72052 RRID#:
Critical Commercial Assays		
RT² Profiler PCR Array Human WNT Signaling Pathway Plus	Qiagen	PAHS-043YC-2
Human Dkk-3 DuoSet Solid Phase Sandwich ELISA	R&D Systems	DY1118

3’ Transcript Capture and Single Cell Library Prep v3 chemistry	10x Genomics	
Visium Spatial Technology slide, starter kit and Library Prep	10x Genomics	1000200
Deposited Data		
Raw and processed scRNAseq data	This paper	GEO: GSE142489
VDR-ChIP sequencing data	PMID: 30905091	GEO: GSE124576
Raw and processed spatial RNAseq data	This paper	GEO: submitted 10.14.2020
Experimental Models: Cell Lines		
Patient-derived Primary Cells	UIC Cancer Center Tissue Bank Core Facility, protocol # 2004-0679	N/A
PC3	ATCC	Cat #: CRL-1435, RRID:CVCL_0035
957E/hTERT	Laboratory of Dr. Donald Vander Griend	RRID:CVCL_X476
RWPE1	ATCC	Cat #: CRL-11609, RRID:CVCL_3791
LAPC4	Laboratory of Dr. Charles Sawyers	Cat# CRL-13009, RRID:CVCL_4744
Experimental Models: Organisms/Strains		
N/A	N/A	N/A
Oligonucleotides		
VDR was quantified using forward primer 5’-GACCTGTGGCAACCAAGACT-3’ and reverse primer 5’- GAACTTGATGAGGGGCTCAA-3’.	This paper	N/A
CYP24A1 was quantified using forward primer 5’-CATTTTAGCAGTCAGCTCCCG-3’ and reverse primer 5’-GGCAACAGTTCTGGGTGAAT-3’	This paper	N/A
DKK3 was quantified using forward primer 5’-TCACATCTGTGGGAGACGAA-3’ and reverse primer 5’-CTGGCAGGTGTACTGGAAGC-3’	This paper	N/A
HPRT1 was quantified using forward primer 5’-TGCTGACCTGCTGGATTACA-3’ and reverse primer 5’-CTGCATTGTTTTGCCAGTGT-3’	This paper	N/A
AXIN2 was quantified using forward primer 5’-AGTGTGAGGTCCACGGAAAC-3’ and reverse primer 5’-ACAGGATCGCTCCTCTTGAA-3’	This paper	N/A
Recombinant DNA		
N/A	N/A	N/A
Software and Algorithms		
CellRanger	10x Genomics	
SpaceRanger	10x Genomics	
Loupe Browser	10x Genomics	
Seurat	Butler et al., 2018; Satija et al., 2015	https://satijalab.org/seurat/
Monocle	Cao et al., 2019; Qiu et al., 2017; Trapnell et al., 2014	https://cole-trapnell-lab.github.io/monocle3/

Other		
VDR siRNA pool	Santa Cruz Biotechnology	Cat #: sc-106692
CTL siRNA pool	Santa Cruz Biotechnology	Cat #: sc-37007

REFERENCES

Baumann, B., et al. (2019). "High levels of PIWI-interacting RNAs are present in the small RNA landscape of prostate epithelium from vitamin D clinical trial specimens." Prostate **79**(8): 840-855.

Blajszczak, C. C. and L. Nonn (2019). "Vitamin D regulates prostate cell metabolism via genomic and non-genomic mitochondrial redox-dependent mechanisms." J Steroid Biochem Mol Biol **195**: 105484.

Butler, A., et al. (2018). "Integrating single-cell transcriptomic data across different conditions, technologies, and species." Nat. Biotech. **36**: 411.

Cao, J., et al. (2019). "The single-cell transcriptional landscape of mammalian organogenesis." Nature **566**(7745): 496-502.

Giangreco, A. A. and L. Nonn (2013). "The sum of many small changes: microRNAs are specifically and potentially globally altered by vitamin D3 metabolites." J. Steroid Biochem. Mol. Biol. **136**: 86-93.

Livak, K. J. and T. D. Schmittgen (2001). "Analysis of relative gene expression data using real-time quantitative PCR and the 2(-Delta Delta C(T)) Method." Methods **25**(4): 402-408.

Maund, S. L., et al. (2014). "Optimization and comprehensive characterization of a faithful tissue culture model of the benign and malignant human prostate." Lab Invest **94**(2): 208-221.

McCray, T., et al. (2019). "Single-cell RNA-Seq analysis identifies a putative epithelial stem cell population in human primary prostate cells in monolayer and organoid culture conditions." Am. J. Clin. Exp. Urol. **7**(3): 123-138.

McCray, T., et al. (2019). "Handling and assessment of human primary prostate organoid culture." J. Vis. Exp.: 1-4.

Nonn, L., et al. (2006). "Inhibition of p38 by vitamin D reduces interleukin-6 production in normal prostate cells via mitogen-activated protein kinase phosphatase 5: implications for prostate cancer prevention by vitamin D." Cancer Res. **66**(8): 4516-4524.

Peehl, D. M. (2003). "Growth of prostatic epithelial and stromal cells in vitro." Methods Mol Med **81**: 41-57.

Qiu, X., et al. (2017). "Reversed graph embedding resolves complex single-cell trajectories." Nat. Methods **14**(10): 979-982.

Richards, Z., et al. (2019). "Prostate stroma increases the viability and maintains the branching phenotype of human prostate organoids." iScience **12**: 304-317.

Satija, R., et al. (2015). "Spatial reconstruction of single-cell gene expression data." Nat. Biotechnol. **33**: 495-502.

Trapnell, C., et al. (2014). "The dynamics and regulators of cell fate decisions are revealed by pseudotemporal ordering of single cells." Nat. Biotechnol. **32**: 381-386.

Xin, L., et al. (2003). "In vivo regeneration of murine prostate from dissociated cell populations of postnatal epithelia and urogenital sinus mesenchyme." Proc. Natl. Acad. Sci. U.S.A. **100 Suppl 1**: 11896-11903.